J|A|C|S
ARTICLES
Published on Web 10/16/2004

Spirocyclic Zwitterionic λ^5*Si*-Silicates with Two Bidentate Ligands Derived from α-Amino Acids or α-Hydroxycarboxylic Acids: Synthesis, Structure, and Stereodynamics

Reinhold Tacke,* Rüdiger Bertermann, Christian Burschka, Simona Dragota, Martin Penka, and Ingo Richter

Contribution from the Institut für Anorganische Chemie, Universität Würzburg, Am Hubland, D-97074 Würzburg, Germany

Received May 11, 2004; E-mail: r.tacke@mail.uni-wuerzburg.de

Abstract: A series of zwitterionic λ^5*Si*-silicates with a (2,2,6,6-tetramethylpiperidinio)methyl group and two identical bidentate ligands derived from glycine, (*S*)-alanine, (*S*)-phenylalanine, glycolic acid, (*S*)-lactic acid, (*S*)-3-phenyllactic acid, or (*S*)-mandelic acid were synthesized and structurally characterized (solution and solid-state NMR spectroscopy; single-crystal X-ray diffraction). The chiral λ^5*Si*-silicates with ligands derived from optically active α-amino acids or α-hydroxycarboxylic acids were isolated as enantiomerically and diastereomerically pure compounds that undergo a (Λ)/(Δ)-epimerization in solution.

Introduction

Several hitherto unknown bonding situations of pentacoordinate silicon have been realized by using the "zwitterion trick"; i.e., the pentacoordinate (formally negatively charged) silicon atom has been incorporated in a molecular framework that also contains a tetracoordinate (formally positively charged) nitrogen atom.[1,2] The zwitterionic λ^5*Si*-silicates **1**[2d] and **2**,[2e] with their *Si*S_4C or *Si*S_2O_2C skeleton, are recent examples of this particular type of compound. Generally, such zwitterionic λ^5*Si*-silicates are characterized by an excellent crystallizability which is very advantageous for their preparation and isolation and for their structural characterization in the solid state (single-crystal X-ray diffraction, solid-state NMR spectroscopy). In addition, most of these compounds studied so far exist in solution as well and therefore could be investigated for their structure and stereodynamics by solution NMR spectroscopy.[1,2]

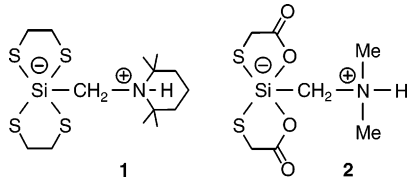

1 **2**

We have now succeeded in synthesizing the first zwitterionic pentacoordinate silicon(IV) complexes that contain two bidentate ligands derived from α-amino acids. We report here on the synthesis of compounds **3**−**5** (zwitterionic λ^5*Si*-silicates with an *Si*O_2N_2C skeleton) that contain ligands derived from glycine, (*S*)-alanine, or (*S*)-phenylalanine. For reasons of comparison, the related compounds **6**−**9** (zwitterionic λ^5*Si*-silicates with an *Si*O_4C framework) were also synthesized (for derivatives of **6**−**9**, see refs 1, 2c,j, and 3). The pairs of compounds **3**/**6**, **4**/**7**, and **5**/**8** represent NH/O analogues. All compounds synthesized contain a protonated 2,2,6,6-tetramethylpiperidino group, which is known to be rather lipophilic. Thus, despite the polar nature of zwitterions, compounds **3**−**9** were expected to be soluble in dichloromethane and trichloromethane and, hence, to be accessible to low-temperature solution NMR studies.

We report here on the synthesis and structural characterization of *rac*-**3**, (Δ,*S*,*S*)-**4** (**4b**), (Λ,*S*,*S*)-**5**·CH_2Cl_2 (**5a**·CH_2Cl_2), *rac*-**6**, (Δ,*S*,*S*)-**7** (**7b**), (Λ,*S*,*S*)-**8**·CH_3CN (**8a**·CH_3CN), and (Λ,*S*,*S*)-**9** (**9a**).[4] All compounds were structurally characterized in the solid

(1) Review dealing with zwitterionic λ^5*Si*-silicates: Tacke, R.; Pülm, M.; Wagner, B. *Adv. Organomet. Chem.* **1999**, *44*, 221−273 and references therein.

(2) Recent original publications dealing with zwitterionic λ^5*Si*-silicates: (a) Kost, D.; Kalikhman, I.; Krivonos, S.; Bertermann, R.; Burschka, C.; Neugebauer, R. E.; Pülm, M.; Willeke, R.; Tacke, R. *Organometallics* **2000**, *19*, 1083−1095. (b) Tacke, R.; Bertermann, R.; Biller, A.; Dannappel, O.; Penka, M.; Pülm, M.; Willeke, R. *Z. Anorg. Allg. Chem.* **2000**, *626*, 1159−1173. (c) Tacke, R.; Ulmer, B.; Wagner, B.; Arlt, M. *Organometallics* **2000**, *19*, 5297−5309. (d) Tacke, R.; Mallak, M.; Willeke, R. *Angew. Chem.* **2001**, *113*, 2401−2403; *Angew. Chem., Int. Ed.* **2001**, *40*, 2339−2341. (e) Willeke, R.; Tacke, R. *Z. Anorg. Allg. Chem.* **2001**, *627*, 1537−1541. (f) Tacke, R.; Bertermann, R.; Dannappel, O.; Neugebauer, R. E.; Pülm, M.; Willeke, R.; Tacke, R. *Inorg. Chem.* **2001**, *40*, 2520−2527. (g) Richter, I.; Burschka, C.; Tacke, R. *J. Organomet. Chem.* **2002**, *646*, 200−203. (h) Richter, I.; Penka, M.; Tacke, R. *Organometallics* **2002**, *21*, 3050−3053. (i) Dragota, S.; Bertermann, R.; Burschka, C.; Heermann, J.; Penka, M.; Richter, I.; Wagner, B.; Tacke, R. *Silicon Chem.* **2002**, *1*, 291−297. (j) Tacke, R.; Bertermann, R.; Biller, A.; Burschka, C.; Penka, M. *Can. J. Chem.* **2003**, *81*, 1315−1325. (k) Bertermann, R.; Biller, A.; Kaupp, M.; Penka, M.; Seiler, O.; Tacke, R. *Organometallics* **2003**, *22*, 4104−4110.

(3) Publications dealing with zwitterionic λ^5*Si*-silicates containing ligands that derive from α-hydroxycarboxylic acids: (a) Tacke, R.; Lopez-Mras, A.; Jones, P. G. *Organometallics* **1994**, *13*, 1617−1623. (b) Mühleisen, M.; Tacke, R. *Organometallics* **1994**, *13*, 3740−3742. (c) Tacke, R.; Mühleisen, M.; Jones, P. G. *Angew. Chem.* **1994**, *106*, 1250−1252; *Angew. Chem., Int. Ed. Engl.* **1994**, *33*, 1186−1188. (d) Mühleisen, M.; Tacke, R. *Chem. Ber.* **1994**, *127*, 1615−1617. (e) Tacke, R.; Heermann, J.; Pülm, M. *Organometallics* **1997**, *16*, 5648−5652. (f) Tacke, R.; Bertermann, R.; Biller, A.; Dannappel, O.; Pülm, M.; Willeke, R. *Eur. J. Inorg. Chem.* **1999**, 795−805. (g) Tacke, R.; Pfrommer, B.; Pülm, M.; Bertermann, R. *Eur. J. Inorg. Chem.* **1999**, 807−816.

(4) Absolute configurations of the compounds studied: *rac*-**3** and *rac*-**6**, racemic mixtures consisting of (Λ)- and (Δ)-enantiomers; **4a**, **5a**, and **7a**-**9a**, (Λ,*S*,*S*)-configuration; **4b**, **5b**, and **7b**-**9b**, (Δ,*S*,*S*)-configuration.

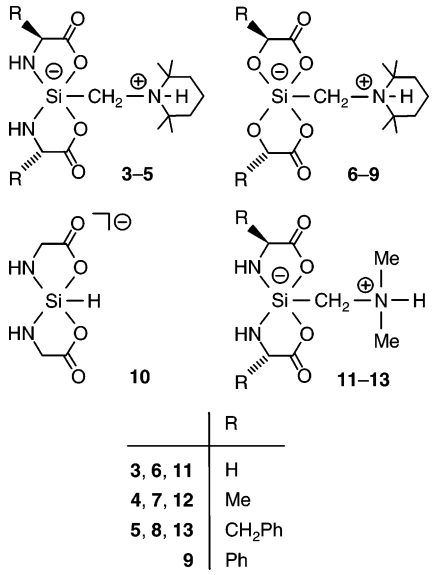

state (crystal structure analyses; ^{15}N and ^{29}Si VACP/MAS NMR experiments) and in solution (^{1}H, ^{13}C, ^{15}N, and ^{29}Si NMR experiments, including studies of the stereodynamics). The experimental investigations were complemented by computational studies of the anionic model species **10** and the zwitterionic model species (Δ)-**11**, (Δ,*S*,*S*)-**12** (**12b**), and (Λ,*S*,*S*)-**13** (**13a**). The investigations presented here were carried out with a special emphasis on the comparison of the respective NH/O analogues. Preliminary results of these studies have been reported elsewhere;[5] for reviews dealing with higher-coordinate silicon compounds, see refs 1 and 6.

Results and Discussion

Syntheses. Compounds **3**−**5** were prepared according to Scheme 1 by treatment of [(2,2,6,6-tetramethylpiperidino)-methyl]silane (**14**)[2d] with 2 molar equiv of glycine, (*S*)-alanine, or (*S*)-phenylalanine. The syntheses were performed in dichloromethane at 20 °C, and compounds *rac*-**3**, **4b**, and **5a**·CH_2Cl_2 were isolated as colorless crystalline solids (yields: *rac*-**3**, 72%; **4b**, 83%; **5a**·CH_2Cl_2, 77%).

Scheme 1

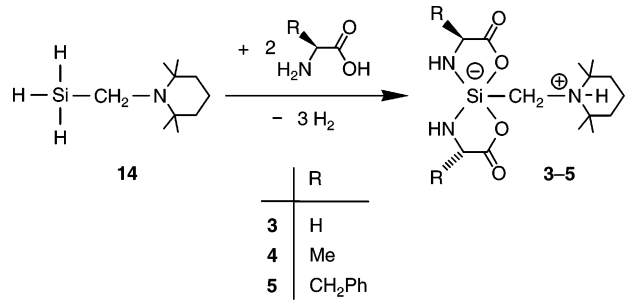

Scheme 2

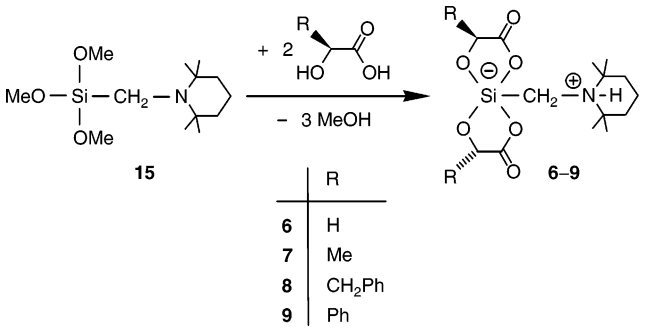

Compounds **6**−**9** were prepared according to Scheme 2 by treatment of trimethoxy[(2,2,6,6-tetramethylpiperidino)methyl]-silane (**15**)[7] with 2 molar equiv of glycolic acid, (*S*)-lactic acid, (*S*)-3-phenyllactic acid, or (*S*)-mandelic acid. The syntheses were performed at 20 °C in methanol (**6**) or acetonitrile (**7**−**9**), and compounds *rac*-**6**, **7b**, **8a**·CH_3CN, and **9a** were isolated as colorless crystalline solids (yields: *rac*-**6**, 80%; **7b**, 91%; **8a**·CH_3CN, 85%; **9a**, 81%).

The resolution of the diastereomers of **4**, **5**, and **7**−**9** by crystallization is quite remarkable, leading to the selective formation of the diastereomerically and enantiomerically pure compounds **4b**, **5a**·CH_2Cl_2, **7b**, **8a**·CH_3CN, and **9a**. In principle, both thermodynamic and kinetic control for this kind of resolution are possible; however, the experimental data available so far do not allow a clear discrimination between these two alternatives.

The identities of *rac*-**3**, **4b**, **5a**·CH_2Cl_2, *rac*-**6**, **7b**, **8a**·CH_3CN, and **9a** were established by elemental analyses (C, H, N), single-crystal X-ray diffraction studies, ^{29}Si VACP/MAS NMR experiments, and solution NMR studies (^{1}H, ^{13}C, ^{15}N, ^{29}Si). Compared to the compounds with an SiO_4C skeleton (*rac*-**6**, **7b**, **8a**·CH_3CN, **9a**), the corresponding analogues with an SiO_2N_2C framework (*rac*-**3**, **4b**, **5a**·CH_2Cl_2) are much more sensitive to water and, hence, more difficult to handle.

Crystal Structure Analyses. The crystal data and the experimental parameters used for the crystal structure analyses of *rac*-**3**, **4b**, **5a**·CH_2Cl_2, *rac*-**6**, **7b**, **8a**·CH_3CN, and **9a** are summarized in Tables 1 and 2. Selected bond distances and angles are listed in Tables 3 and 4. The molecular structures of the zwitterions are depicted in Figures 1−7.

Compounds *rac*-**3** and *rac*-**6** crystallize in the space group *Pbca* and $P2_1/n$, respectively, and the crystals are built up by

(5) Dragota, S.; Bertermann, R.; Burschka, C.; Tacke, R. *13th International Symposium on Organosilicon Chemistry−35th Organosilicon Symposium*; Guanajuato, Mexico, August 25−30, 2002; Abstract P2-46, p 162.

(6) Selected reviews dealing with higher-coordinate silicon compounds: (a) Tandura, S. N.; Voronkov, M. G.; Alekseev, N. V. *Top. Curr. Chem.* **1986**, *131*, 99−189. (b) Sheldrick, W. S. In *The Chemistry of Organic Silicon Compounds*; Patai, S., Rappoport, Z., Eds.; Wiley: Chichester, U.K., 1989; Part 1, pp 227−303. (c) Bassindale, A. R.; Taylor, P. G. In *The Chemistry of Organic Silicon Compounds*; Patai, S., Rappoport, Z., Eds.; Wiley: Chichester, U.K., 1989; Part 1, pp 839−892. (d) Corriu, R. J. P.; Young, J. C. In *The Chemistry of Organic Silicon Compounds*; Patai, S., Rappoport, Z., Eds.; Wiley: Chichester, U.K., 1989; Part 2, pp 1241−1288. (e) Holmes, R. R. *Chem. Rev.* **1990**, *90*, 17−31. (f) Chuit, C.; Corriu, R. J. P.; Reye, C.; Young, J. C. *Chem. Rev.* **1993**, *93*, 1371−1448. (g) Tacke, R.; Becht, J.; Lopez-Mras, A.; Sperlich, J. *J. Organomet. Chem.* **1993**, *446*, 1−8. (h) Wong, C. Y.; Woollins, J. D. *Coord. Chem. Rev.* **1994**, *130*, 175−241. (i) Verkade, J. G. *Coord. Chem. Rev.* **1994**, *137*, 233−295. (j) Tacke, R.; Dannappel, O. In *Tailor-made Silicon-Oxygen Compounds−From Molecules to Materials*; Corriu, R., Jutzi, P., Eds.; Vieweg: Braunschweig, Wiesbaden, Germany, 1996; pp 75−86. (k) Lukevics, E.; Pudova, O. A. *Chem. Heterocycl. Compd. (Engl. Transl.)* **1996**, *32*, 1381−1418. (l) Holmes, R. R. *Chem. Rev.* **1996**, *96*, 927−950. (m) Kost, D.; Kalikhman, I. In *The Chemistry of Organic Silicon Compounds*; Rappoport, Z., Apeloig, Y., Eds.; Wiley: Chichester, U.K., 1998; Vol. 2, Part 2, pp 1339−1445. (n) Pestunovich, V.; Kirpichenko, S.; Voronkov, M. In *The Chemistry of Organic Silicon Compounds*; Rappoport, Z., Apeloig, Y., Eds.; Wiley: Chichester, U.K., 1998; Vol. 2, Part 2, pp 1447−1537. (o) Chuit, C.; Corriu, R. J. P.; Reye, C. In *Chemistry of Hypervalent Compounds*; Akiba, K., Ed.; Wiley-VCH: New York, 1999; pp 81−146. (p) Brook, M. A. *Silicon in Organic, Organometallic, and Polymer Chemistry*; Wiley: New York, 2000; pp 97−114. (q) Tacke, R.; Seiler, O. In *Silicon Chemistry: From the Atom to Extended Systems*; Jutzi, P., Schubert, U., Eds.; Wiley-VCH: Weinheim, Germany, 2003; pp 324−337.

(7) Tacke, R.; Becht, J.; Dannappel, O.; Ahlrichs, R.; Schneider, U.; Sheldrick, W. S.; Hahn, J.; Kiesgen, F. *Organometallics* **1996**, *15*, 2060−2077.

Table 1. Crystal Data and Experimental Parameters for the Crystal Structure Analyses of *rac*-**3**, **4b**, and **5a**·CH_2Cl_2

	rac-**3**	**4b**	**5a**·CH_2Cl_2
empirical formula	$C_{14}H_{27}N_3O_4Si$	$C_{16}H_{31}N_3O_4Si$	$C_{29}H_{41}Cl_2N_3O_4Si$
formula mass (g mol^{-1})	329.48	357.53	594.64
collection T (K)	173(2)	173(2)	173(2)
λ(Mo Kα) (Å)	0.710 73	0.710 73	0.710 73
crystal system	orthorhombic	orthorhombic	monoclinic
space group (no.)	*Pbca* (61)	$P2_12_12_1$ (19)	$P2_1$ (4)
a (Å)	13.458(3)	9.2403(10)	10.809(4)
b (Å)	11.899(2)	10.7313(10)	12.027(4)
c (Å)	20.511(4)	18.712(2)	12.922(4)
β (deg)	90	90	112.89(4)
V (Å^3)	3284.7(11)	1855.5(3)	1547.5(9)
Z	8	4	2
D(calcd) (g cm^{-3})	1.333	1.280	1.276
μ (mm^{-1})	0.165	0.151	0.286
F(000)	1424	776	632
crystal dimensions (mm)	0.6 × 0.4 × 0.3	0.5 × 0.5 × 0.4	0.5 × 0.3 × 0.2
2θ range (deg)	3.98−49.50	4.36−53.98	4.10−52.80
index ranges	$-15 \le h \le 15$, $-13 \le k \le 13$, $-24 \le l \le 24$	$-10 \le h \le 11$, $-13 \le k \le 13$, $-23 \le l \le 23$	$-13 \le h \le 13$, $-15 \le k \le 15$, $-16 \le l \le 16$
no. of collected reflections	27 792	13 428	17 381
no. of independent reflections	2791	3998	6311
R_{int}	0.1486	0.0274	0.0600
no. of reflections used	2791	3998	6311
no. of restraints	0	0	25
no. of parameters	212	232	386
S[a]	0.853	1.045	1.056
weight parameters a/b[b]	0.0281/0.0000	0.0420/0.3523	0.0762/1.3425
$R1$[c] ($I > 2\sigma(I)$)	0.0392	0.0280	0.0530
$wR2$[d] (all data)	0.0763	0.0741	0.1541
absolute structure parameter		−0.04(9)	0.05(9)
max/min residual electron density (e Å^{-3})	+0.196/−0.236	+0.224/−0.185	+0.544/−0.272

[a] $S = \{\Sigma[w(F_o^2 - F_c^2)^2]/(n-p)\}^{0.5}$; n = no. of reflections; p = no. of parameters. [b] $w^{-1} = \sigma^2(F_o^2) + (aP)^2 + bP$, with $P = [\max(F_o^2,0) + 2F_c^2]/3$. [c] $R1 = \Sigma||F_o| - |F_c||/\Sigma|F_o|$. [d] $wR2 = \{\Sigma[w(F_o^2 - F_c^2)^2]/\Sigma[w(F_o^2)^2]\}^{0.5}$.

(Λ)- and (Δ)-enantiomers. All the other compounds crystallize in chiral space groups (Tables 1 and 2), and the crystals investigated contain only one particular diastereomer.

The *Si*-coordination polyhedra of *rac*-**3**, **4b**, and **5a**·CH_2Cl_2 (compounds with an *Si*O_2N_2C skeleton) are distorted trigonal bipyramids, with the oxygen atoms O1 and O2 in the axial positions. The nitrogen atoms N1 and N2 and the carbon atom C1 occupy the equatorial sites. The Si−O distances range from 1.8129(10) Å to 1.8356(19) Å, and the Si−C bond lengths are in the range 1.906(3)−1.918(2) Å. These values are similar to the axial Si−O distances and the equatorial Si−C distances, respectively, observed for the related compounds *rac*-**6**, **7b**, **8a**·CH_3CN, and **9a** (see below). The Si−N distances range from 1.713(2) Å to 1.725(3) Å. As expected, these values are slightly longer than the equatorial Si−O distances of *rac*-**6**, **7b**, **8a**·CH_3CN, and **9a** (see below).

The *Si*-coordination polyhedra of *rac*-**6**, **7b**, **8a**·CH_3CN, and **9a** (compounds with an *Si*O_4C framework) are also distorted trigonal bipyramids, with the carboxylato oxygen atoms O1 and O3 in the axial positions. The alcoholato oxygen atoms O2 and O4 and the carbon atom C1 occupy the equatorial sites. The Si−O distances range from 1.659(2) Å to 1.8131(11) Å, the axial Si−O bonds (1.787(2)−1.8131(11) Å) being significantly longer than the equatorial ones (1.659(2)−1.6667(11) Å). The Si−C bond lengths are in the range 1.8949(16)−1.9090(17) Å. Generally, the Si−O and the Si−C distances are similar to those reported for related zwitterionic *λ*^{5}*Si*-silicates with *Si*O_4C skeletons and ligands derived from α-hydroxycarboxylic acids (in this context, see refs 1, 2c,j, and 3).

In conclusion, the bond distances and angles of the respective NH/O analogues *rac*-**3**/*rac*-**6**, **4b**/**7b**, and **5a**·CH_2Cl_2/**8a**·CH_3CN are characterized by distinct similarities. This could point to similar bonding situations in the analogous *Si*O_2N_2C and *Si*O_4C skeletons.

As can be seen from Figures 1−7 and Table 5, all compounds studied form an intramolecular N−H···O hydrogen bond between the ammonium NH group and one of the two axial oxygen atoms.[8] The respective axial Si−O bonds (Si−O1) containing the hydrogen acceptor atom (O1) are slightly longer than the other axial Si−O bonds (Si−O2 (*Si*O_2N_2C) or Si−O3 (*Si*O_4C)). In the case of compounds *rac*-**3** and **4b**, an additional intermolecular N−H···O interaction between one of the two SiNH groups and one of the two carbonyl oxygen atoms was observed.[8] This hydrogen bond leads to the formation of chains in the crystals of *rac*-**3** and **4b** (Figures 8 and 9).[9]

NMR Studies. Compounds *rac*-**3**, **4b**, **5a**·CH_2Cl_2, *rac*-**6**, **7b**, **8a**·CH_3CN, and **9a** were characterized at 22 °C by solid-state ^{29}Si VACP/MAS NMR spectroscopy (Table 6). The isotropic ^{29}Si chemical shifts obtained clearly characterize the ^{29}Si resonance signals as arising from pentacoordinate silicon atoms, the chemical shifts of the respective NH/O analogues being very similar. The solid-state ^{29}Si NMR spectra of *rac*-**6**, **7b**, **8a**·CH_3CN, and **9a** (compounds with an *Si*O_4C skeleton) are characterized by sharp resonance signals (full-width at half-height ca. 15−25 Hz), whereas the resonance signals of *rac*-**3**, **4b**, and **5a**·CH_2Cl_2 (compounds with an *Si*O_2N_2C skeleton) are split or are broad (only slightly structured) due to $^1J(^{14}N,^{29}Si)$ couplings. We were not able to simulate these spectra and to extract the $^1J(^{14}N,^{29}Si)$ coupling constants because these couplings were poorly resolved. The line width of the ^{29}Si signals depends on the magnitude of $^1J(^{14}N,^{29}Si)$ and the quadrupole relaxation time of the ^{14}N nucleus Tq(^{14}N). When Tq(^{14}N) becomes comparable with $1/^1J(^{14}N,^{29}Si)$, splitting of the ^{29}Si resonance signals due to ^{14}N,^{29}Si coupling can be observed directly.[10]

All zwitterionic *λ*^{5}*Si*-silicates were characterized at 22 °C by solid-state ^{15}N VACP/MAS NMR spectroscopy (see Experimental Section). The spectra obtained were compatible with the crystal structures of these compounds and demonstrated that the nonracemic compounds **4b**, **5a**·CH_2Cl_2, **7b**, **8a**·CH_3CN, and **9a** were diastereomerically and enantiomerically pure. The isotropic ^{15}N chemical shifts were very similar to those obtained in the solution ^{15}N NMR studies, indicating that the zwitterions exist in solution as well.

(8) The hydrogen-bonding systems were analyzed by using the program system PLATON: Spek, A. L. *PLATON*; University of Utrecht: Utrecht, The Netherlands, 1998.

(9) In the case of **4b**, an additional intermolecular N1−H1···O3 interaction could be discussed (N1−H 0.888 Å, H···O3 2.637 Å, N1···O3 3.405 Å, N1−H···O3 145.21°) that leads to a cross-linkage of the chains built up by the N2−H···O4 hydrogen bonds to give a two-dimensional network. However, the H···O3 distance is slightly longer than the default cutoff value implemented in the program system PLATON.

(10) Kupče, E.; Lukevics, E. *J. Magn. Reson.* **1988**, *76*, 63−73.

Table 2. Crystal Data and Experimental Parameters for the Crystal Structure Analyses of *rac*-**6**, **7b**, **8a**·CH_3CN, and **9a**

	rac-**6**	**7b**	**8a**·CH_3CN	**9a**
empirical formula	$C_{14}H_{25}NO_6Si$	$C_{16}H_{29}NO_6Si$	$C_{30}H_{40}N_2O_6Si$	$C_{26}H_{33}NO_6Si$
formula mass (g mol^{-1})	331.44	359.49	552.73	483.62
collection T (K)	173(2)	173(2)	173(2)	173(2)
λ(Mo Kα) (Å)	0.710 73	0.710 73	0.710 73	0.710 73
crystal system	monoclinic	tetragonal	monoclinic	orthorhombic
space group (no.)	$P2_1/n$ (14)	$P4_1$ (76)	$P2_1$ (4)	$P2_12_12_1$ (19)
a (Å)	7.765(2)	8.0232(10)	11.0878(15)	10.878(4)
b (Å)	16.084(3)	8.0232(10)	11.2514(12)	11.036(3)
c (Å)	13.204(3)	28.688(3)	12.8474(17)	20.267(10)
β (deg)	103.32(3)	90	113.727(15)	90
V (Å^3)	1604.7(6)	1846.7(4)	1467.3(3)	2433.1(16)
Z	4	4	2	4
D(calcd) (g cm^{-3})	1.372	1.293	1.251	1.320
μ (mm^{-1})	0.175	0.157	0.125	0.139
F(000)	712	776	592	1032
crystal dimensions (mm)	0.2 × 0.2 × 0.2	0.5 × 0.4 × 0.4	0.5 × 0.3 × 0.1	0.3 × 0.3 × 0.2
2θ range (deg)	5.06−49.46	5.08−47.90	5.02−52.90	4.20−46.66
index ranges	$-9 \le h \le 8$, $-18 \le k \le 18$, $-15 \le l \le 15$	$-9 \le h \le 8$, $-8 \le k \le 9$, $-32 \le l \le 31$	$-13 \le h \le 13$, $-14 \le k \le 14$, $-16 \le l \le 16$	$-12 \le h \le 12$, $-12 \le k \le 11$, $-22 \le l \le 22$
no. of collected reflections	20 477	6805	16 615	9830
no. of independent reflections	2731	2832	6021	3504
R_{int}	0.0648	0.0269	0.0624	0.0768
max/min transmission	0.9659/0.9659			
no. of reflections used	2731	2832	6021	3504
no. of restraints	0	1	1	0
no. of parameters	208	226	360	314
S^a	0.934	1.034	1.013	0.979
weight parameters a/b^b	0.0544/0.0000	0.0501/0.0000	0.0493/0.0000	0.0464/0.0000
$R1^c$ ($I > 2\sigma(I)$)	0.0336	0.0259	0.0324	0.0385
$wR2^d$ (all data)	0.0836	0.0667	0.0821	0.0884
absolute structure parameter		−0.05(10)	−0.03(8)	−0.10(15)
extinction coefficient	0.0043(10)			
max/min residual electron density (e Å^{-3})	+0.172/−0.242	+0.156/−0.137	+0.172/−0.243	+0.182/−0.262

[a] $S = \{\Sigma[w(F_o^2 - F_c^2)^2]/(n-p)\}^{0.5}$; n = no. of reflections; p = no. of parameters. [b] $w^{-1} = \sigma^2(F_o^2) + (aP)^2 + bP$, with $P = [\max(F_o^2,0) + 2F_c^2]/3$. [c] $R1 = \Sigma||F_o| - |F_c||/\Sigma|F_o|$. [d] $wR2 = \{\Sigma[w(F_o^2 - F_c^2)^2]/\Sigma[w(F_o^2)^2]\}^{0.5}$.

Table 3. Selected Bond Distances (Å) and Angles (deg) for *rac*-**3**, **4b**, and **5a**·CH_2Cl_2

	rac-**3**	**4b**	**5a**·CH_2Cl_2
Si−O1	1.8356(19)	1.8294(10)	1.835(2)
Si−O2	1.8163(19)	1.8129(10)	1.817(3)
Si−N1	1.717(2)	1.7150(13)	1.725(3)
Si−N2	1.713(2)	1.7146(13)	1.725(3)
Si−C1	1.918(2)	1.9157(14)	1.906(3)
O1−Si−O2	176.25(9)	178.50(5)	175.81(12)
O1−Si−N1	86.45(10)	86.93(5)	86.41(13)
O1−Si−N2	90.94(10)	93.30(5)	91.76(13)
O1−Si−C1	93.58(9)	92.55(5)	94.47(13)
O2−Si−N1	91.64(10)	93.23(5)	91.18(14)
O2−Si−N2	87.60(10)	87.80(6)	86.98(14)
O2−Si−C1	90.15(9)	86.06(5)	89.68(13)
N1−Si−N2	126.59(11)	126.76(6)	127.31(16)
N1−Si−C1	115.30(11)	118.06(6)	117.40(16)
N2−Si−C1	118.10(11)	115.11(7)	115.25(16)

Compounds *rac*-**3**, **4b**, **5a**·CH_2Cl_2, *rac*-**6**, **7b**, **8a**·CH_3CN, and **9a** were additionally characterized by solution ^{1}H, ^{13}C, and ^{29}Si NMR spectroscopy. Furthermore, 2D ^{15}N,^{1}H HMQC NMR spectra were recorded for *rac*-**3**, **4b**, and **5a**·CH_2Cl_2. All these solution NMR studies were performed at 23 °C using CD_2Cl_2 or $CDCl_3$ (*rac*-**6** only) as the solvent. As can be seen from Table 6, the ^{29}Si chemical shifts are very similar to the isotropic ^{29}Si chemical shifts obtained in the solid-state NMR experiments, indicating that the λ^5*Si*-silicate skeletons of all these compounds exist in solution as well. Furthermore, the ^{1}H chemical shifts observed for the $SiCH_2NH$ protons ($\delta = 5.7-6.0$ ppm) indicate the presence of the ammonium moieties. Thus, these NMR experiments unequivocally demonstrate that the zwitterions also exist in solution (for further details, see Experimental Section).

As the trigonal-bipyramidal structure, with the carboxylato oxygen atoms in the axial sites, is the energetically most favorable one for all the zwitterionic λ^5*Si*-silicates studied (see Crystal Structure Analyses and Computational Studies), it is likely that this particular structure is also dominant in solution. The chiral nature of the zwitterions is reflected by the ABX spin systems observed for the $SiCH_AH_BNH_X$ protons in the ^{1}H NMR spectra. In the case of *rac*-**3** and *rac*-**6** (*chiral* λ^5*Si*-silicate skeletons with *achiral* bidentate ligands), diastereotopism of the $SiCH_AH_BN$ protons indicates that these zwitterions are configurationally stable on the NMR time scale at 23 °C. It is likely that all the other compounds studied (*chiral* λ^5*Si*-silicate skeletons with *chiral* bidentate ligands) are also configurationally stable on the NMR time scale at 23 °C, but this information cannot be extracted directly from the ^{1}H NMR spectra because the chiral nature of the configurationally stable bidentate ligands ((*S*)-configuration) could already be sufficient for the existence of ABX spin systems for the $SiCH_AH_BNH_X$ protons; i.e., the ABX spin systems observed cannot be correlated exclusively with the chirality of the λ^5*Si*-silicate skeletons ((Λ)- and (Δ)-configuration) of **4**, **5**, and **7**−**9**.

Upon dissolution of **4b**, **5a**·CH_2Cl_2, **7b**, **8a**·CH_3CN, and **9a**, a (Λ)/(Δ)-epimerization was observed. This isomerization process leads to equilibrium mixtures of the respective diastereomers (**4a** ⇄ **4b**; **5a** ⇄ **5b**; **7a** ⇄ **7b**; **8a** ⇄ **8b**; **9a** ⇄ **9b**). It is

Table 4. Selected Bond Distances (Å) and Angles (deg) for *rac*-**6**, **7b**, **8a**·CH_3CN, and **9a**

	rac-**6**	7b	**8a**·CH_3CN	9a
Si−O1	1.8127(12)	1.8077(11)	1.8131(11)	1.811(2)
Si−O2	1.6633(13)	1.6624(12)	1.6667(11)	1.666(2)
Si−O3	1.7901(13)	1.7875(11)	1.8017(12)	1.787(2)
Si−O4	1.6664(13)	1.6643(12)	1.6654(11)	1.659(2)
Si−C1	1.9006(19)	1.9090(17)	1.8949(16)	1.896(3)
O1−Si−O2	89.11(6)	88.96(5)	88.72(5)	88.94(10)
O1−Si−O3	175.74(6)	178.32(6)	176.22(5)	179.51(10)
O1−Si−O4	87.74(6)	90.97(5)	90.15(5)	90.18(10)
O1−Si−C1	93.72(7)	92.45(6)	94.08(6)	92.84(11)
O2−Si−O3	89.19(6)	89.47(5)	88.19(5)	90.57(10)
O2−Si−O4	123.29(7)	119.94(7)	124.49(6)	120.70(11)
O2−Si−C1	118.16(7)	121.60(7)	119.65(6)	121.28(12)
O3−Si−O4	89.94(6)	90.32(6)	89.82(5)	90.14(10)
O3−Si−C1	90.52(7)	87.87(6)	89.33(6)	87.35(11)
O4−Si−C1	118.55(8)	118.40(7)	115.79(7)	117.98(12)

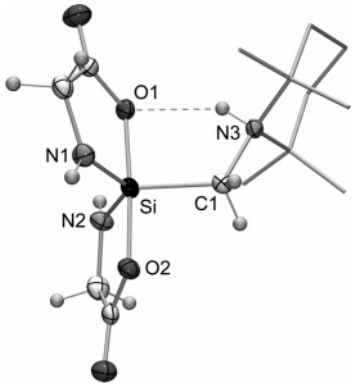

Figure 1. Molecular structure of *rac*-**3** ((Δ)-enantiomer) in the crystal (probability level of displacement ellipsoids 50%; tetramethylpiperidinio group represented as stick model).

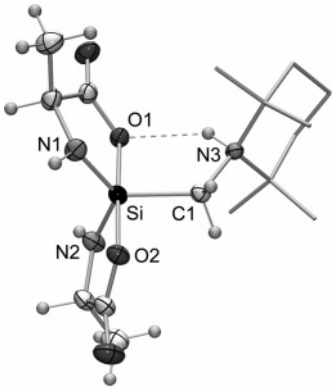

Figure 2. Molecular structure of **4b** ((Δ,*S*,*S*)-diastereomer) in the crystal (probability level of displacement ellipsoids 50%; tetramethylpiperidinio group represented as stick model).

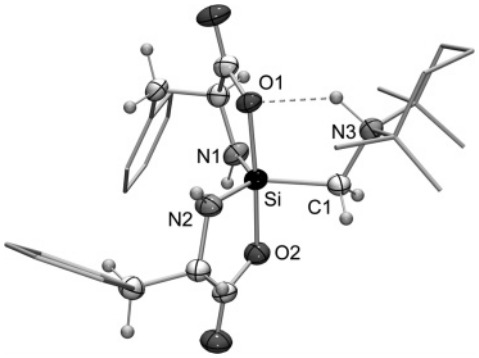

Figure 3. Molecular structure of **5a** ((Λ,*S*,*S*)-diastereomer) in the crystal of **5a**·CH_2Cl_2 (probability level of displacement ellipsoids 50%; tetramethylpiperidinio and phenyl groups represented as stick models).

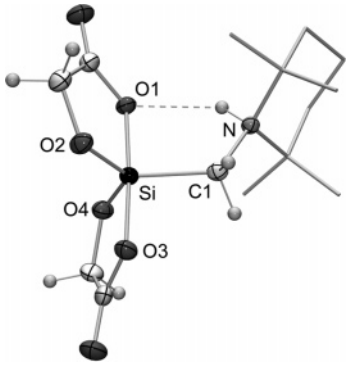

Figure 4. Molecular structure of *rac*-**6** ((Δ)-enantiomer) in the crystal (probability level of displacement ellipsoids 50%; tetramethylpiperidinio group represented as stick model).

likely that the enantiomers of **3** and **6** undergo an analogous (Λ)/(Δ)-enantiomerization. In the case of **4** and **5** (compounds with an *Si*O_2N_2C skeleton), the absolute configurations of the respective diastereomers in solution could be assigned because the kinetics of the epimerization process at the silicon atom upon dissolution of **4b** and **5a**·CH_2Cl_2 in CD_2Cl_2 could be monitored by ^{1}H NMR spectroscopy (see below). In the case of **7**−**9** (compounds with an *Si*O_4C skeleton), the absolute configurations of the diastereomers could not be assigned because the epimerization process was too fast and could not be monitored by ^{1}H NMR spectroscopy; even upon dissolution of **7b**, **8a**·CH_3CN, and **9a** in CD_2Cl_2 at −60 °C, a spontaneous equilibration was observed. Thus, the zwitterionic λ^5*Si*-silicates with an *Si*O_4C skeleton are significantly less configurationally stable than their analogues with an *Si*O_2N_2C framework.

The kinetics of the epimerization processes **4a** ⇄ **4b** and **5a** ⇄ **5b** were studied at 23 °C by ^{1}H NMR spectroscopy at 300.1 MHz. For this purpose, the diastereomerically and enantiomerically pure compounds **4b** and **5a**·CH_2Cl_2 were dissolved in CD_2Cl_2 (**4b**, c = 30 mmol L^{-1}; **5a**·CH_2Cl_2, c = 78 mmol L^{-1}), and the integrals of the NC*H*C_2 resonance signals of the two bidentate ligands of **4a**/**4b** and **5a**/**5b** were measured as a function of time. The first ^{1}H NMR spectra were recorded 5 and 6 min, respectively, after dissolution of **4b** and **5a**·CH_2Cl_2 and revealed already partial epimerization, with the following molar ratios: **4a**/**4b**, 0.23:0.77; **5a**/**5b**, 0.95:0.05. To follow the epimerization processes, ^{1}H NMR spectra were recorded every 300 and 135 s, respectively. After a period of ca. 2 and ca. 3 h,

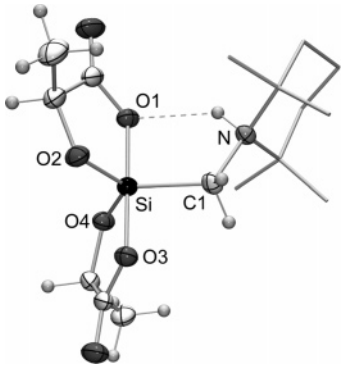

Figure 5. Molecular structure of **7b** ((Δ,*S*,*S*)-diastereomer) in the crystal (probability level of displacement ellipsoids 50%; tetramethylpiperidinio group represented as stick model).

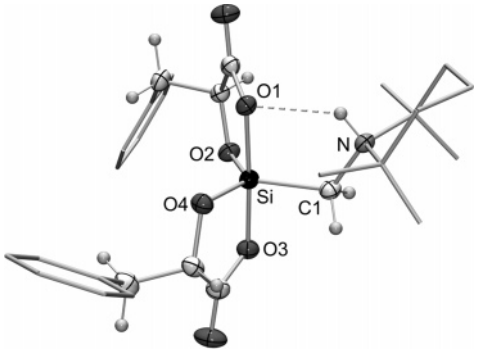

Figure 6. Molecular structure of **8a** ((Λ,*S*,*S*)-diastereomer) in the crystal of **8a**·CH_3CN (probability level of displacement ellipsoids 50%; tetramethylpiperidinio and phenyl groups represented as stick models).

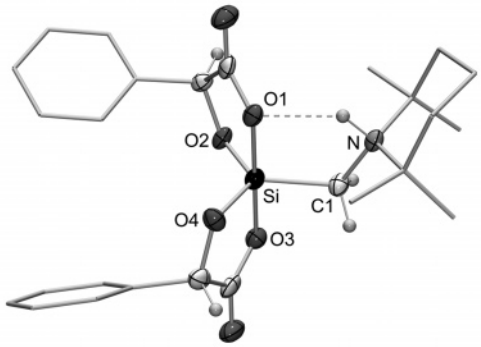

Figure 7. Molecular structure of **9a** ((Λ,*S*,*S*)-diastereomer) in the crystal (probability level of displacement ellipsoids 50%; tetramethylpiperidinio and phenyl groups represented as stick model).

Table 5. Hydrogen-Bonding Geometries for *rac*-**3**, **4b**, **5a**·CH_2Cl_2, *rac*-**6**, **7b**, **8a**·CH_3CN, and **9a** in the Crystal[8,9]

	D–H···A	D–H (Å)	H···A (Å)	D···A (Å)	D–H···A (deg)
rac-**3**	N2–H···O4 (inter)	0.87(4)	2.42(3)	3.183(3)	146(3)
	N3–H···O1 (intra)	0.87(2)	2.06(3)	2.770(3)	138(2)
4b	N2–H···O4 (inter)	0.833(19)	2.589(19)	3.3350(19)	149.9(18)
	N3–H···O1 (intra)	0.900(17)	2.112(17)	2.7955(15)	132.0(14)
5a·CH_2Cl_2	N3–H···O1 (intra)	1.05(5)	1.98(4)	2.807(4)	133(3)
rac-**6**	N–H···O1 (intra)	0.88(2)	2.13(2)	2.776(2)	129.9(18)
7b	N–H···O1 (intra)	0.89(2)	2.07(2)	2.7463(17)	133(2)
8a·CH_3CN	N–H···O1 (intra)	0.87(2)	2.197(19)	2.8202(17)	128.7(16)
9a	N–H···O1 (intra)	0.96(3)	1.98(3)	2.732(3)	134(2)

respectively, the equilibration was completed, with the following molar equilibrium ratios: **4a**/**4b**, 0.71:0.29; **5a**/**5b**, 0.73:0.27. These data indicate that the energy differences between the respective (Λ,*S*,*S*)- and (Δ,*S*,*S*)-diastereomers are small, the

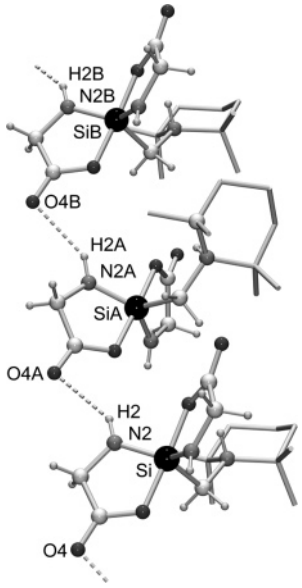

Figure 8. Intermolecular N–H···O hydrogen bonds in the crystal of *rac*-**3** leading to infinite chains along the base [0 1 0] vector (tetramethylpiperidinio groups represented as stick model).[8]

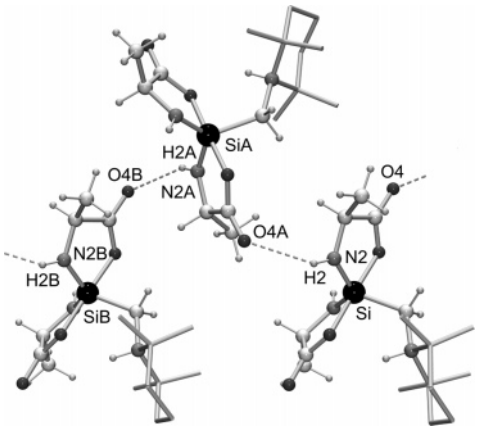

Figure 9. Intermolecular N–H···O hydrogen bonds in the crystal of **4b** leading to infinite chains along the base [1 0 0] vector (tetramethylpiperidinio groups represented as stick model).[8,9]

Table 6. ^{29}Si NMR Data for *rac*-**3**, **4b**, **5a**·CH_2Cl_2, *rac*-**6**, **7b**, **8a**·CH_3CN, and **9a** in the Crystal and in Solution[a]

	δ (crystal)[b]	δ (solution)
rac-**3**	−94.1 to −91.8 (m)	−91.9[c]
4b	−100.5 to −98.0 (m)	−97.1 (**4a**)/−98.4 (**4b**)[c]
5a·CH_2Cl_2	−98.5 to −96.0 (m)	−97.36 (**5a**)/−97.45 (**5b**)[c]
rac-**6**	−89.3	−91.6[d]
7b	−96.6	−96.3/−97.5[c]
8a·CH_3CN	−95.3	−96.5[c]
9a	−94.5	−95.9/−96.4 [c]

[a] Spectra recorded at 22 °C (solid state) or 23 °C (solution); chemical shifts in ppm. [b] Isotropic chemical shifts obtained by solid-state ^{29}Si VACP/MAS NMR experiments. [c] Solvent CD_2Cl_2 (*rac*-**3**, c = 81 mmol L^{-1}; **4b**, c = 30 mmol L^{-1}; **5a**·CH_2Cl_2, c = 78 mmol L^{-1}; **7b**, c = 56 mmol L^{-1}; **8a**·CH_3CN, c = 48 mmol L^{-1}; **9a**, c = 41 mmol L^{-1}). [d] Solvent $CDCl_3$ (*rac*-**6**, c = 121 mmol L^{-1}).

(Λ,*S*,*S*)-isomers being somewhat more stable than the corresponding (Δ,*S*,*S*)-epimers. It is interesting to note that the more stable (Λ,*S*,*S*)-epimer is also found in the crystal of **5a**·CH_2Cl_2, whereas crystalline **4b** contains the less stable (Δ,*S*,*S*)-epimer. The kinetics of the epimerization processes studied are depicted in Figures 10 and 11. In these figures, the percentages

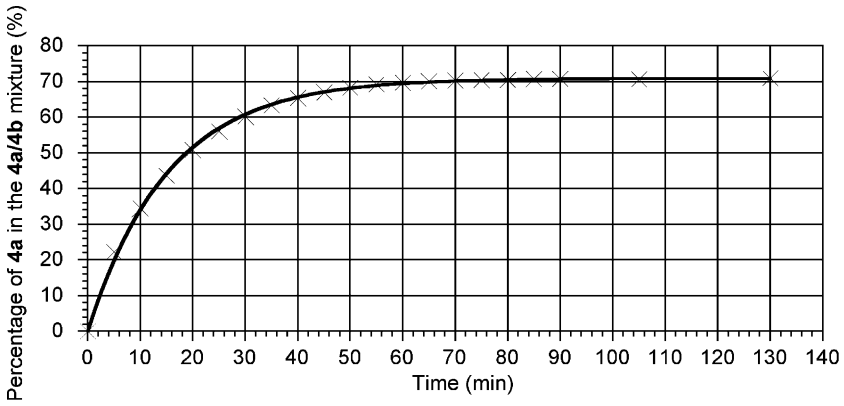

Figure 10. Kinetics of the epimerization process of **4a** ⇄ **4b** after dissolution of **4b** in CD_2Cl_2 (c = 30 mmol L^{-1}). The experimental data were extracted from ^1H NMR spectra (23 °C, 300.1 MHz). The solid line represents a fit of the experimental curve with the monoexponential equation $f(t) = m_1[1 - \exp(-t/m_2)]$, with $m_1 = 70.9 \pm 0.2$ and $m_2 = 15.4 \pm 0.2$.

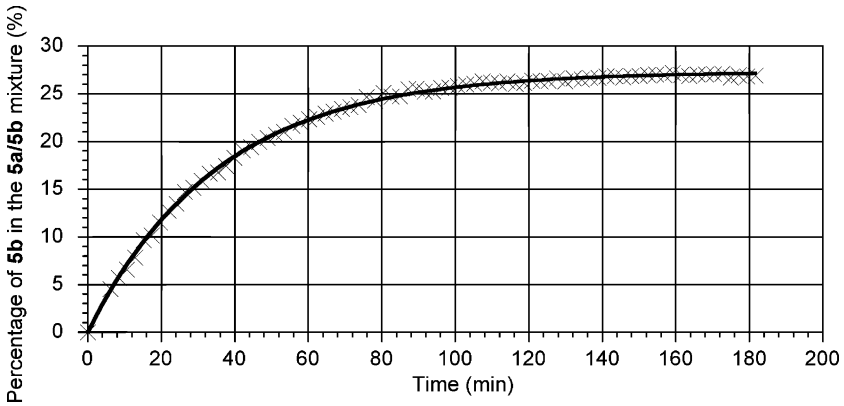

Figure 11. Kinetics of the epimerization process of **5a** ⇄ **5b** after dissolution of **5a**·CH_2Cl_2 in CD_2Cl_2 (c = 78 mmol L^{-1}). The experimental data were extracted from ^1H NMR spectra (23 °C, 300.1 MHz). The solid line represents a fit of the experimental curve with the monoexponential equation $f(t) = m_1[1 - \exp(-t/m_2)]$, with $m_1 = 27.3 \pm 0.1$ and $m_2 = 35.5 \pm 0.2$.

of **4a** and **5b** in the respective mixtures of epimers are plotted against the time. The experimental curves could be fitted with a monoexponential function of the type $f(t) = m_1[1 - \exp(-t/m_2)]$.

The kinetics of the epimerization process **4a** ⇄ **4b** were additionally studied by VT ^1H NMR experiments at 300.1 MHz in the temperature range −60 °C to 0 °C using CD_2Cl_2 as the solvent. For this purpose, a sample of diastereomerically and enantiomerically pure **4b** was dissolved in CD_2Cl_2 at different temperatures, and ^1H NMR spectra were recorded every 300 s (monitoring of the epimerization process by integration of the respective NC*H*C_2 resonance signals). Compound **4b** was found to be configurationally stable at −60 °C and −40 °C: no changes of the NMR spectra were observed over a period of ca. 24 h. However, upon dissolution of **4b** at −20 °C, a very slow epimerization process took place which was partially monitored at this particular temperature over a period of ca. 32 h, revealing the following molar ratio after that period: **4a**/**4b**, 0.27:0.73. After dissolution of **4b** at −10 °C, ^1H NMR spectra were recorded over a period of ca. 67 h, leading to the following molar ratio: **4a**/**4b**, 0.61:0.39. According to analogous kinetic studies at 0 °C, the thermodynamic equilibrium was reached after ca. 4 h (molar equilibrium ratio: **4a**/**4b**, 0.71:0.29). A comparison of the kinetics of the epimerization processes studied at −20 °C, −10 °C, and 0 °C is depicted in Figure 12, in which the percentages of **4a** in the respective mixtures of epimers are plotted against the time. The experimental curves could be fitted with a monoexponential function of the type $f(t) = m_1[1 - \exp(-t/m_2)]$.

In conclusion, the NH/O analogues **4b**/**7b** and **5a**/**8a** differ substantially in their configurational stability in solution, the compounds with ligands derived from α-amino acids being much more stable. It is an open question as to whether the mechanism for the (Λ)/(Δ)-isomerization of **3**−**5** (SiO_2N_2C skeletons) is identical with that for the (Λ)/(Δ)-isomerization of **6**−**9** (SiO_4C skeletons; for studies concerning the mechanism of the (Λ)/(Δ)-isomerization of chiral zwitterionic λ^5*Si*-silicates with an SiO_4C framework closely related to **6**−**9**, see refs 2j, 3f).

Computational Studies. To obtain more information about the structure of the zwitterions **3**, **4b**, and **5a**, quantum-chemical investigations were performed. For this purpose, computational studies of the anionic model species **10** (SCF/TZP+ level) and the zwitterionic model species (Δ)-**11**, **12b**, and **13a** (SCF/TZP level) were carried out. These zwitterions represent derivatives of **3**, **4b**, and **5a**, with a dimethylammonio group instead of the 2,2,6,6-tetramethylpiperidinio moiety. The results of quantum-chemical studies of related zwitterionic λ^5*Si*-silicates with bidentate ligands derived from α-hydroxycarboxylic acids (compounds with an SiO_4C skeleton) have already been reported elsewhere.[2j,3f]

As shown in Figure 13, four different structures (**10A**−**10D**) were studied for the anionic model species **10**. For energetic reasons, square pyramids with the hydrogen atom in a basal

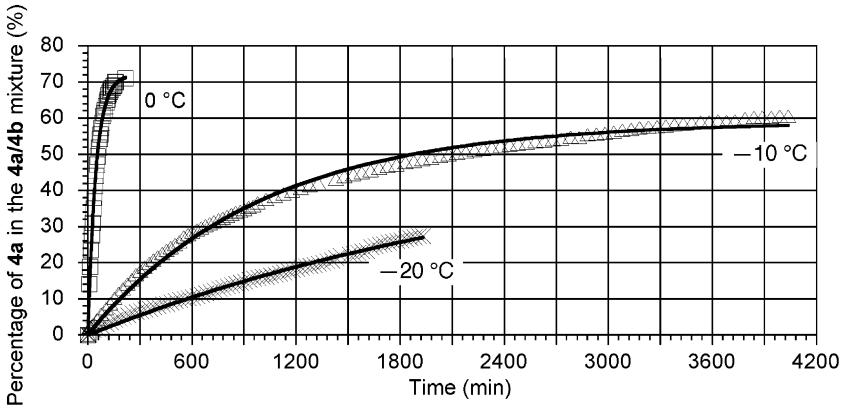

Figure 12. Comparison of the kinetics of the epimerization process of **4a** ⇄ **4b** after dissolution of **4b** in CD_2Cl_2 ($c = 30$ mmol L^{-1}) at different temperatures. The experimental data were extracted from ^1H NMR spectra (300.1 MHz). The solid lines represent fits of the experimental curves with monoexponential equations of the type $f(t) = m_1[1 - \exp(-t/m_2)]$; −20 °C, $m_1 = 54.5 \pm 3.0$, $m_2 = 2825 \pm 197.0$; −10 °C, $m_1 = 59.0 \pm 0.4$, $m_2 = 997 \pm 18.2$; 0 °C, $m_1 = 71.9 \pm 0.5$, $m_2 = 46.9 \pm 1.0$. The errors of the fit for the experiment at −20 °C are relatively large because only the beginning of the epimerization process was observed due to its long duration.

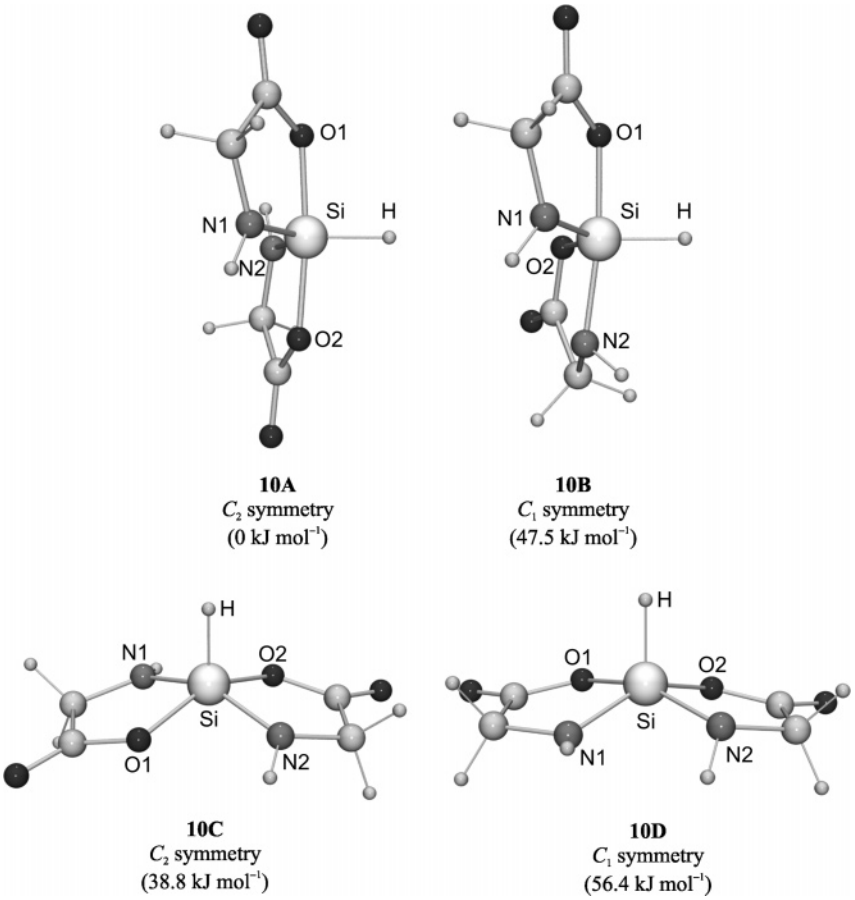

Figure 13. Calculated structures and relative energies of **10A** and **10B** (local minima), **10C** (a geometry nearby the expected Berry-type square-pyramidal transition state), and **10D** (transition state) as obtained by SCF/TZP+ geometry optimizations. **10C** does not represent a stationary point (the gradient does not vanish); however, test calculations indicate that the potential energy surface in the vicinity of this particular geometry is quite flat. The anion **10D** with a possible C_s symmetry does not represent a critical point.

position were not considered. The trigonal-bipyramidal species **10A** and **10B** and the square-pyramidal species **10C** are chiral and therefore exist as (Λ)- and (Δ)-enantiomers. Calculations of the vibrational frequencies demonstrated that **10A** and **10B** represent local minima (a third possible minimum, with both nitrogen atoms occupying the axial sites, could not be located as a stationary point), whereas **10C** represents a geometry nearby the expected Berry-type square-pyramidal transition state (no stationary point; the sum of the basal angles had to be fixed in internal coordinates during the geometry optimization), and **10D** is a transition state (for selected geometric parameters for **10A**−**10D**, see Table 7). The trigonal-bipyramidal structure, with the two oxygen atoms in the axial sites, is the energetically most favorable one. This result is in agreement with the experimentally established structures of the *Si*-coordination polyhedra in the crystals of *rac*-**3**, **4b**, and **5a**·CH_2Cl_2. The energy barrier between the trigonal-bipyramidal local minima **10A** and **10B** and **10C** and **10D** are relatively high (38.8 and 56.4 kJ mol^{-1},

Table 7. Selected Calculated Bond Distances (Å) and Angles (deg) for the Local Minima **10A** and **10B**, for the Idealized Geometry **10C**, and for the Transition State **10D** as Obtained by SCF/TZP+ Geometry Optimizations

	10A	10B	10C	10D
Si−O1	1.818	1.821	1.798	1.790
Si−O2	1.818	1.725	1.798	1.764
Si−N1	1.730	1.731	1.759	1.771
Si−N2	1.730	1.827	1.759	1.795
Si−H	1.479	1.488	1.483	1.482
O1−Si−O2	173.6	87.7	150.8	84.4
O1−Si−N1	85.7	85.0	85.1	84.4
O1−Si−N2	91.4	171.9	87.9	157.4
O1−Si−H	93.2	89.7	104.6	97.9
O2−Si−N1	91.4	126.0	87.9	145.6
O2−Si−N2	85.7	86.5	85.1	86.4
O2−Si−H	93.2	113.0	104.6	102.5
N1−Si−N2	125.7	93.9	151.8	91.7
N1−Si−H	117.1	120.4	104.1	111.3
N2−Si−H	117.1	97.7	104.1	104.2

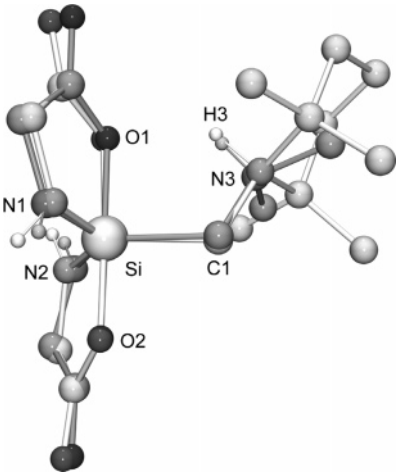

Figure 14. Superposition of the calculated structure of the zwitterion (Δ)-**11** (darker bonds and atoms) and the experimentally established structure (brighter bonds and atoms) of (Δ)-**3**. The hydrogen atoms (except for NH) are omitted for clarity.

respectively), indicating that Berry-type distortions of the trigonal-bipyramidal *Si*-coordination polyhedra of **3**, **4b**, and **5a**·CH_2Cl_2 cannot be achieved as easy as those in related zwitterionic λ^5*Si*-silicates with an SiO_4C skeleton and bidentate ligands derived from α-hydroxycarboxylic acids (in this context, see refs 2j, 3f).

Based on the structure of the energetically most favorable species **10A**, geometry optimizations at the SCF/TZP level were carried out for the zwitterions (Δ)-**11**, **12b**, and **13a** (Figures 14−16). As can be seen from Table 8, the calculated interatomic distances and angles for the SiO_2N_2C frameworks of these model species are in reasonable agreement with the respective data obtained in the crystal structure analyses of *rac*-**3**, **4b**, and **5a**·CH_2Cl_2. The discrepancies observed between the calculated and experimentally established structures may be explained by intermolecular interactions in the crystal, including intermolecular hydrogen bonds in the case of *rac*-**3** and **4b**.

The results obtained in the computational studies of **10** suggest that the energetically preferred trigonal-bipyramidal *Si*-coordination polyhedra of **3**, **4b**, and **5a**, with the oxygen atoms in the axial sites, also play the major role in solution. However, further species, such as square-pyramidal Berry-type species

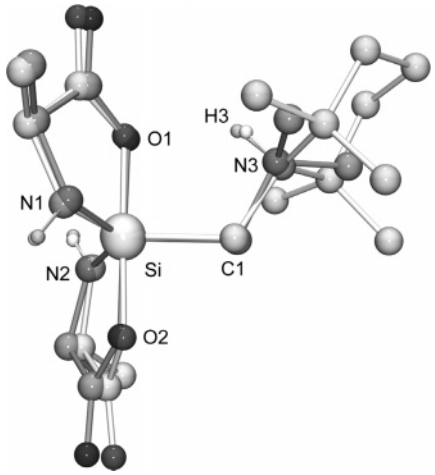

Figure 15. Superposition of the calculated structure of the zwitterion **12b** (darker bonds and atoms) and the experimentally established structure (brighter bonds and atoms) of **4b**. The hydrogen atoms (except for NH) are omitted for clarity.

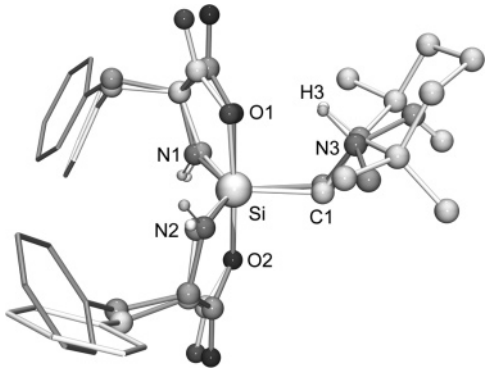

Figure 16. Superposition of the calculated structure of **13a** (darker bonds and atoms) and the experimentally established structure (brighter bonds and atoms) of **5a**. The hydrogen atoms (except for NH) are omitted for clarity, and the phenyl rings are represented as stick models.

Table 8. Selected Calculated Bond Distances (Å) and Angles (deg) for (Δ)-**11**, **12b**, and **13a**

	(Δ)-11	12b	13a
Si−O1	1.829	1.823	1.825
Si−O2	1.759	1.760	1.759
Si−N1	1.716	1.716	1.715
Si−N2	1.726	1.725	1.721
Si−C1	1.944	1.942	1.947
O1−Si−O2	179.5	179.4	179.5
O1−Si−N1	85.5	85.3	85.5
O1−Si−N2	92.2	92.6	92.3
O1−Si−C1	88.8	90.1	88.9
O2−Si−N1	94.1	95.0	94.1
O2−Si−N2	88.1	87.6	87.9
O2−Si−C1	91.3	89.2	91.4
N1−Si−N2	128.3	127.1	128.9
N1−Si−C1	116.9	117.9	116.5
N2−Si−C1	114.7	115.0	114.6

(analogous to **10C**), may also play a certain role in solution at room temperature.

Experimental Section

General Procedures. The syntheses were carried out under dry nitrogen. The organic solvents used were dried and purified according to standard procedures and stored under nitrogen. Melting points were determined with a Büchi melting point B-540 apparatus using samples

in sealed capillaries. The ^{1}H, ^{13}C, ^{15}N, and ^{29}Si solution NMR spectra were recorded on a Bruker DRX-300 NMR spectrometer (^{1}H, 300.1 MHz; ^{13}C, 75.5 MHz; ^{15}N, 30.4 MHz; ^{29}Si, 59.6 MHz). CD_2Cl_2 (99.6% D, <0.01% H_2O) or $CDCl_3$ (99.96% D, <0.005% H_2O) were used as the solvents (Euriso-top). Chemical shifts (ppm) were determined relative to internal $CDHCl_2$ (^{1}H, δ 5.32; CD_2Cl_2), internal $CHCl_3$ (^{1}H, δ 7.24; $CDCl_3$), internal CD_2Cl_2 (^{13}C, δ 53.8; CD_2Cl_2), internal $CDCl_3$ (^{13}C, δ 77.0; $CDCl_3$), external formamide (^{15}N, δ −268.0; CD_2Cl_2), or external TMS (^{29}Si, δ 0; CD_2Cl_2, $CDCl_3$). Analysis and assignment of the ^{1}H NMR data were supported by ^{1}H,^{1}H COSY and ^{13}C,^{1}H, ^{15}N,^{1}H, and ^{29}Si,^{1}H correlation experiments, and the ^{1}H spin systems were analyzed by using the program WIN-DAISY 4.05.[11] The $^{2}J_{AB}$ coupling constants reported for the AB parts of the spin systems studied represent absolute values. Assignment of the ^{13}C NMR data was supported by DEPT 135 experiments. The thermocouple used with the probe in the VT ^{1}H NMR experiments was calibrated for low temperatures according to ref 12 using a 4% solution of CH_3OH in CD_3OD. The VT ^{1}H NMR spectra were recorded in the temperature range −60 °C to 23 °C; the time required for temperature equilibration was 15 min. Solid-state ^{15}N and ^{29}Si VACP/MAS NMR spectra were recorded at 22 °C on a Bruker DSX-400 NMR spectrometer with bottom layer rotors of ZrO_2 (diameter 7 mm) containing ca. 300 mg of sample (^{15}N, 40.6 MHz; ^{29}Si, 79.5 MHz; external standard, TMS (^{29}Si, δ = 0) or glycine (^{15}N, δ = −342.0); spinning rate, 5−7 kHz; contact time, 3 ms (^{15}N) or 5 ms (^{29}Si); 90° ^{1}H transmitter pulse length, 3.6 μs; repetition time, 4 s).

Preparation of *rac*-Bis[glycinato(2−)-*N*,*O*][(2,2,6,6-tetramethylpiperidinio)methyl]silicate (*rac*-3). Compound **14** (2.00 g, 10.8 mmol) was added at 20 °C to a stirred suspension of glycine (1.62 g, 21.6 mmol) in dichloromethane (10 mL), and the mixture was stirred at this temperature for 24 h (evolution of hydrogen). The remaining solid was separated by filtration and discarded, *n*-pentane (25 mL) was added to the filtrate, and the resulting solution was kept undisturbed at −20 °C for 48 h (formation of crystals). The precipitate was isolated by filtration and dried in vacuo (0.01 Torr, 60 °C, 2 days) to give *rac*-**3** in 72% yield as a colorless crystalline product (2.56 g, 7.77 mmol); mp 162 °C (dec). ^{15}N VACP/MAS NMR (22 °C, ν_{rot} = 5 kHz) δ −353.1 (SiNHC), −352.4 (SiNHC), −290.6 (C_3NH); ^{29}Si VACP/MAS NMR (22 °C, ν_{rot} = 5 kHz) δ −94.1 to −91.8 (m). ^{1}H NMR (CD_2Cl_2, c = 81 mmol L^{-1}, 23 °C) δ 1.28 (br s, 2 H, SiNHC), 1.30 (s, 3 H, CCH_3), 1.33 (s, 6 H, CCH_3), 1.49 (s, 3 H, CCH_3), 1.53−1.92 (m, 6 H, CCH_2C), 2.37 (δ_A) and 2.62 (δ_B) (AB part of an ABX system, $^{2}J_{AB}$ = 16.5 Hz, $^{3}J_{AX}$ = 3.9 Hz, $^{3}J_{BX}$ = 3.5 Hz, 2 H, $SiCH_AH_BNH_X$), 3.44 (δ_A) and 3.59 (δ_B) (AB part of an ABX system, $^{2}J_{AB}$ = 16.9 Hz, $^{3}J_{AX}$ = 0.7 Hz, $^{3}J_{BX}$ = 2.0 Hz, 4 H, $CCH_AH_BNH_XSi$), 5.8 (br s, 1 H, C_3NH); ^{13}C NMR (CD_2Cl_2, c = 81 mmol L^{-1}, 23 °C) δ 16.0 (NCC*C*H$_2$C), 20.1 (C*C*H$_3$), 20.3 (C*C*H$_3$), 29.8 (C*C*H$_3$), 30.9 (C*C*H$_3$), 39.5 (NC*C*H$_2$C), 39.7 (NC*C*H$_2$C), 40.5 (SiCH$_2$N), 46.5 (NCH$_2$C), 65.1 (NC*C*$_3$), 65.4 (N*C*C$_3$), 176.1 (C═O); ^{15}N NMR (CD_2Cl_2, c = 81 mmol L^{-1}, 23 °C) δ −357.5 (SiNHC), −298.5 (C_3NH); ^{29}Si NMR (CD_2Cl_2, c = 81 mmol L^{-1}, 23 °C) δ −91.9. Anal. Calcd for $C_{14}H_{27}N_3O_4Si$: C, 51.04; H, 8.26; N, 12.75. Found: C, 50.3; H, 7.8; N, 11.8.[13]

Preparation of (Δ,*S*,*S*)-Bis[alaninato(2−)-*N*,*O*][(2,2,6,6-tetramethylpiperidinio)methyl]silicate (4b). Compound **14** (500 mg, 2.70 mmol) was added at 20 °C to a stirred suspension of (*S*)-alanine (481 mg, 5.40 mmol) in dichloromethane (8 mL), and the mixture was stirred at this temperature for 48 h (evolution of hydrogen). The remaining solid was separated by filtration and discarded, *n*-pentan (30 mL) was added to the filtrate, and the resulting solution was kept undisturbed at −20 °C for 24 h (formation of crystals). The precipitate was isolated by filtration and dried in vacuo (0.01 Torr, 60 °C, 2 days) to give **4b** in 83% yield as a colorless crystalline product (800 mg, 2.24 mmol); mp 250 °C (dec). ^{15}N VACP/MAS NMR (22 °C, ν_{rot} = 5 kHz) δ −334.3 (2 N, SiNHC), −290.3 (C_3NH); ^{29}Si VACP/MAS NMR (22 °C, ν_{rot} = 5 kHz) δ −100.5 to −98.0 (m). Upon dissolution of **4b** in CD_2Cl_2 (c = 30 mmol L^{-1}) at 23 °C, epimerization occurred (establishment of an equilibrium, with a molar ratio **4a**/**4b** = 0.71:0.29). NMR data for **4a**: ^{1}H NMR (CD_2Cl_2, 23 °C) δ, 1.24 (d, $^{3}J_{HH}$ = 6.8 Hz, 6 H, NCHC*H*$_3$), 1.30 (s, 3 H, CCH_3), 1.32 (s, 6 H, CCH_3), 1.38 (br s, 2 H, SiNHC), 1.49 (s, 3 H, CCH_3), 1.56−1.92 (m, 6 H, CCH_2C), 2.35 (δ_A) and 2.60 (δ_B) (AB part of an ABX system, $^{2}J_{AB}$ = 16.4 Hz, $^{3}J_{AX}$ = 3.8 Hz, $^{3}J_{BX}$ = 3.5 Hz, 2 H, $SiCH_AH_BNH_X$), 3.56 (q, $^{3}J_{HH}$ = 6.8 Hz, 2 H, NC*H*CH$_3$), 5.9 (br s, 1 H, C_3NH); ^{13}C NMR (CD_2Cl_2, 23 °C) δ 16.0 (NCC*C*H$_2$C), 20.1 (C*C*H$_3$), 20.3 (C*C*H$_3$), 23.6 (NCH*C*H$_3$), 30.0 (C*C*H$_3$), 31.0 (C*C*H$_3$), 39.5 (NC*C*H$_2$C), 39.7 (NC*C*H$_2$C), 40.6 (SiCH$_2$N), 52.4 (N*C*HCH$_3$), 64.9 (N*C*C$_3$), 65.3 (NC*C*$_3$), 178.9 (C═O); ^{15}N NMR (CD_2Cl_2, 23 °C) δ −337.5 (SiNHC), −298.5 (C_3NH); ^{29}Si NMR (CD_2Cl_2, 23 °C) δ −97.1. NMR data for **4b**: ^{1}H NMR (CD_2Cl_2, 23 °C) δ, 1.19 (d, $^{3}J_{HH}$ = 6.8 Hz, 6 H, NCHC*H*$_3$), 1.32 (s, 6 H, CCH_3), 1.34 (s, 3 H, CCH_3), 1.39 (br s, 2 H, SiNHC), 1.55 (s, 3 H, CCH_3), 1.56−1.92 (m, 6 H, CCH_2C), 2.33 (δ_A) and 2.68 (δ_B) (AB part of an ABX system, $^{2}J_{AB}$ = 16.5 Hz, $^{3}J_{AX}$ = 3.9 Hz, $^{3}J_{BX}$ = 3.3 Hz, 2 H, $SiCH_AH_BNH_X$), 3.76 (A part of an AMX_3 system, $^{3}J_{AX}$ = 6.8 Hz, $^{3}J_{AM}$ = 2.1 Hz, 2 H, $H_MNCH_AC(H_x)_3$), 6.0 (br s, 1 H, C_3NH); ^{13}C NMR (CD_2Cl_2, 23 °C) δ 16.0 (NCC*C*H$_2$C), 20.1 (C*C*H$_3$), 20.4 (C*C*H$_3$), 21.9 (NCH*C*H$_3$), 31.4 (C*C*H$_3$), 31.6 (C*C*H$_3$), 39.6 (NC*C*H$_2$C), 39.7 (NC*C*H$_2$C), 41.5 (SiCH$_2$N), 51.6 (N*C*HCH$_3$), 64.9 (N*C*C$_3$), 65.1 (NC*C*$_3$), 178.7 (C═O); ^{15}N NMR (CD_2Cl_2, 23 °C) δ −337.5 (SiNHC), −299.5 (C_3NH); ^{29}Si NMR (CD_2Cl_2, 23 °C) −98.4. Anal. Calcd for $C_{16}H_{31}N_3O_4Si$: C, 53.75; H, 8.74; N, 11.75. Found: C, 53.0; H, 8.5; N, 11.6.[13]

Preparation of (Λ,*S*,*S*)-Bis[phenylalaninato(2−)-*N*,*O*][(2,2,6,6-tetramethylpiperidinio)methyl]silicate−Dichloromethane (5a·CH_2Cl_2). Compound **14** (1.00 g, 5.39 mmol) was added at 20 °C to a stirred suspension of (*S*)-phenylalanine (1.78 g, 10.8 mmol) in dichloromethane (15 mL), and the mixture was stirred at this temperature for 48 h (evolution of hydrogen). The remaining solid was separated by filtration and discarded, *n*-pentane (35 mL) was added to the filtrate, and the resulting solution was kept undisturbed at 20 °C for 6 h (formation of crystals). The precipitate was isolated by filtration and dried in a nitrogen gas stream (20 °C, 1 h) to give **5a**·CH_2Cl_2 in 77% yield as a colorless crystalline solid (2.47 g, 4.15 mmol); mp 193 °C (dec).^{15}N VACP/MAS NMR (22 °C, ν_{rot} = 5 kHz) δ −335.6 (SiNHC), −334.7 (SiNHC), −291.7 (C_3NH); ^{29}Si VACP/MAS NMR (22 °C, ν_{rot} = 5 kHz) δ −98.5 to −96.0 (m). Upon dissolution of **5a**·CH_2Cl_2 in CD_2Cl_2 (c = 78 mmol L^{-1}) at 23 °C, epimerization occurred (establishment of an equilibrium, with a molar ratio **5a**/**5b** = 0.73:0.27). NMR data for **5a**: ^{1}H NMR (CD_2Cl_2, 23 °C) δ 1.27 (s, 3 H, CCH_3), 1.30 (s, 6 H, CCH_3), 1.40 (s, 3 H, CCH_3), 1.44 (br s, 2 H, SiNHC), 1.55−1.95 (m, 6 H, CCH_2C), 2.33 (δ_A) and 2.57 (δ_B) (AB part of an ABX system, $^{2}J_{AB}$= 16.6 Hz, $^{3}J_{AX}$ = 3.8 Hz, $^{3}J_{BX}$ = 3.5 Hz, 2 H, $SiCH_AH_BNH_X$), 2.58 (δ_A), 3.22 (δ_B), and 3.71 (δ_X) (ABX system, $^{2}J_{AB}$ = 13.1 Hz, $^{3}J_{AX}$ = 9.9 Hz, $^{3}J_{BX}$ = 3.3 Hz, 6 H, $CCH_AH_BCH_X$), 5.8 (br s, 1 H, C_3NH), 7.13−7.36 (m, 10 H, C_6H_5); ^{13}C NMR (CD_2Cl_2, 23 °C) δ 16.0 (NCC*C*H$_2$C), 20.1 (C*C*H$_3$), 20.3 (C*C*H$_3$), 30.0 (C*C*H$_3$), 31.1 (C*C*H$_3$), 39.6 (NC*C*H$_2$C), 39.7 (NC*C*H$_2$C), 40.7 (SiCH$_2$N), 44.0 (NCH*C*H$_2$C), 58.7 (N*C*HCH$_2$C), 65.0 (N*C*C$_3$), 65.3 (N*C*C$_3$), 126.6 (C4, C_6H_5), 128.8 (C2/C6, C_6H_5), 129.7 (C3/C5, C_6H_5), 139.7 (C1, C_6H_5), 177.3 (C═O); ^{15}N NMR (CD_2Cl_2, 23 °C) δ −344.0 (SiNHC), −297.5 (C_3NH); ^{29}Si NMR (CD_2Cl_2, 23 °C) δ −97.36. NMR data for **5b**: ^{1}H NMR (CD_2Cl_2, 23 °C) δ 1.30 (s, 3 H, CCH_3), 1.31 (br s, 2 H, SiNHC), 1.35 (s, 3 H, CCH_3), 1.42 (s, 3 H, CCH_3), 1.46 (s, 3 H, CCH_3), 1.55−1.95 (m, 6 H, CCH_2C), 2.25 (δ_A) and 2.67 (δ_B) (AB part of an ABX system, $^{2}J_{AB}$ = 16.5 Hz, $^{3}J_{AX}$ = 3.9 Hz, $^{3}J_{BX}$ = 3.4 Hz, 2 H, $SiCH_AH_BNH_X$), 2.44 (δ_A), 3.19 (δ_B), and 3.83 (δ_X) (ABX part of an ABXY system, $^{2}J_{AB}$ =

(11) (a) Program WIN-DAISY 4.05; Bruker-Franzen GmbH: Bremen, Germany, 1998. (b) Weber, U.; Germanus, A.; Thiele, H. *Fresenius J. Anal. Chem.* **1997**, *359*, 46−49.

(12) Braun, S.; Kalinowski, H.-O.; Berger, S. *150 and More Basic NMR Experiments*; Wiley-VCH: Weinheim, Germany, 1998; pp 136−139.

(13) Apart from some remaining dichloromethane (solvent for the synthesis), the sample was NMR-spectroscopically pure. The dichloromethane could not be totally removed in vacuo at 60 °C, and drying at higher temperatures resulted in a partial decomposition. These problems, together with the hydrolytic sensitivity of the sample, are responsible for the unsatisfactory results obtained in the elemental analyses.

13.2 Hz, $^3J_{AX}$ = 10.0 Hz, $^3J_{BX}$ = 3.3 Hz, $^3J_{XY}$ = 1.6 Hz, 6 H, CCH_AH_B-CH_XNH_Y), 5.9 (br s, 1 H, C_3NH), 7.13−7.36 (m, 10 H, C_6H_5); ^{13}C NMR (CD_2Cl_2, 23 °C) δ 16.0 (NCC*C*H$_2$C), 20.2 (C*C*H$_3$), 20.4 (C*C*H$_3$), 31.6 (C*C*H$_3$), 31.7 (C*C*H$_3$), 39.6 (NC*C*H$_2$C), 39.8 (NC*C*H$_2$C), 41.1 (SiCH$_2$N), 42.0 (NCHCH$_2$C), 58.0 (N*C*HCH$_2$C), 65.0 (N*C*C$_3$), 65.2 (N*C*C$_3$), 126.5 (C4, C_6H_5), 128.8 (C2/C6, C_6H_5), 129.5 (C3/C5, C_6H_5), 140.1 (C1, C_6H_5), 177.1 (C═O); ^{15}N NMR (CD_2Cl_2, 23 °C) δ −345.0 (SiNHC), −297.5 (C_3NH); ^{29}Si NMR (CD_2Cl_2, 23 °C) −97.45. Anal. Calcd for $C_{29}H_{41}Cl_2N_3O_4Si$: C, 58.58; H, 6.95; N, 7.07. Found: C, 58.2; H, 6.7; N, 7.0.

Preparation of *rac*-Bis[glycolato(2−)-*O*^{1},*O*^{2}][(2,2,6,6-tetramethylpiperidinio)methyl]silicate (*rac*-6). Compound **15** (831 mg, 3.02 mmol) was added at 20 °C to a stirred solution of glycolic acid (459 mg, 6.04 mmol) in methanol (10 mL), and the mixture was stirred at this temperature for 48 h. The resulting precipitate was isolated by filtration, recrystallized from boiling methanol (slow cooling of a saturated solution to 20 °C), washed with cold methanol (0 °C, 2 × 3 mL), and dried in vacuo (0.01 Torr, 20 °C, 3 h) to give *rac*-**6** in 80% yield as a colorless crystalline solid (800 mg, 2.41 mmol); mp 270 °C. ^{15}N VACP/MAS NMR (22 °C, ν_{rot} = 5 kHz) δ −290.7 (C_3NH); ^{29}Si VACP/MAS NMR (22 °C, ν_{rot} = 7 kHz) δ −89.3. ^1H NMR ($CDCl_3$, c = 121 mmol L^{-1}, 23 °C) δ 1.28 (s, 3 H, CCH_3), 1.34 (s, 3 H, CCH_3), 1.35 (s, 3 H, CCH_3), 1.48 (s, 3 H, CCH_3), 1.64−1.92 (m, 6 H, CCH_2C), 2.47 (δ_A) and 2.74 (δ_B) (AB part of an ABX system, $^2J_{AB}$ = 17.4 Hz, $^3J_{AX}$ = 4.2 Hz, $^3J_{BX}$ = 3.4 Hz, 2 H, $SiCH_AH_BNH_X$), 4.06 (δ_A) and 4.24 (δ_B) (AB system, $^2J_{AB}$ = 16.6 Hz, 4 H, OCH_AH_BC), 5.9 (br s, 1 H, NH); ^{13}C NMR ($CDCl_3$, c = 121 mmol L^{-1}, 23 °C) δ 15.6 (NCC*C*H$_2$C), 19.9 (C*C*H$_3$), 20.2 (C*C*H$_3$), 29.6 (C*C*H$_3$), 30.2 (C*C*H$_3$), 37.0 (SiCH$_2$N), 38.8 (NC*C*H$_2$C), 38.9 (NC*C*H$_2$C), 63.9 (O*C*H$_2$C), 65.4 (N*C*C$_3$), 65.9 (N*C*C$_3$), 174.6 (C═O); ^{29}Si NMR ($CDCl_3$, c = 121 mmol L^{-1}, 23 °C) δ −91.6. Anal. Calcd for $C_{14}H_{25}NO_6Si$: C, 50.73; H, 7.60; N, 4.23. Found C, 50.7; H, 7.7; N, 4.1.

Preparation of (Δ,*S*,*S*)-Bis[lactato(2−)-*O*^{1},*O*^{2}][(2,2,6,6-tetramethylpiperidinio)methyl]silicate (7b). Compound **15** (500 mg, 1.82 mmol) was added at 20 °C to a stirred solution of (*S*)-lactic acid (328 mg, 3.64 mmol) in acetonitrile (1 mL), and the mixture was stirred for 1 min and then kept undisturbed at this temperature for 1 h. The resulting precipitate was isolated by filtration, washed with acetonitrile (4 × 5 mL), and dried in vacuo (0.01 Torr, 20 °C, 4 h) to give **7b** in 91% yield as a colorless crystalline solid (592 mg, 1.65 mmol); mp 278 °C. ^{15}N VACP/MAS NMR (22 °C, ν_{rot} = 5 kHz) δ −290.3 (C_3NH); ^{29}Si VACP/MAS NMR (22 °C, ν_{rot} = 5 kHz) δ −96.6. Upon dissolution of **7b** in CD_2Cl_2 (c = 56 mmol L^{-1}) at 23 °C, epimerization occurred (establishment of an equilibrium, with a molar ratio major isomer/minor isomer = 0.77:0.23). NMR data for the major isomer: ^1H NMR (CD_2Cl_2, 23 °C) δ 1.27 (s, 3 H, CCH_3), 1.33 (s, 3 H, CCH_3), 1.34 (s, 3 H, CCH_3), 1.35 (d, $^3J_{HH}$ = 7.0 Hz, 6 H, OCHC*H*$_3$), 1.46 (s, 3 H, CCH_3), 1.62−1.92 (m, 6 H, CCH_2C), 2.46 (δ_A) and 2.71 (δ_B) (AB part of an ABX system, $^2J_{AB}$ = 17.3 Hz, $^3J_{AX}$ = 4.0 Hz, $^3J_{BX}$ = 3.2 Hz, 2 H, $SiCH_AH_BNH_X$), 4.16 (q, $^3J_{HH}$ = 7.0 Hz, 2 H, OC*H*CH$_3$), 5.9 (br s, 1 H, NH); ^{13}C NMR (CD_2Cl_2, 23 °C) δ 15.9 (NCC*C*H$_2$C), 20.1 (C*C*H$_3$), 20.3 (C*C*H$_3$), 20.7 (OCH*C*H$_3$), 29.9 (C*C*H$_3$), 30.4 (C*C*H$_3$), 37.4 (SiCH$_2$N), 39.3 (NC*C*H$_2$C), 39.5 (NC*C*H$_2$C), 65.7 (N*C*C$_3$), 66.1 (N*C*C$_3$), 70.7 (O*C*HCH$_3$), 177.3 (C═O); ^{29}Si NMR (CD_2Cl_2, 23 °C) δ −96.3. NMR data for the minor isomer: ^1H NMR (CD_2Cl_2, 23 °C) δ 1.31 (s, 3 H, CCH_3), 1.32 (d, $^3J_{HH}$ = 7.0 Hz, 6 H, OCHC*H*$_3$), 1.35 (s, 3 H, CCH_3), 1.40 (s, 3 H, CCH_3), 1.50 (s, 3 H, CCH_3), 1.62−1.92 (m, 6 H, CCH_2C), 2.44 (δ_A) and 2.79 (δ_B) (AB part of an ABX system, $^2J_{AB}$ = 17.4 Hz, $^3J_{AX}$ = 4.1 Hz, $^3J_{BX}$ = 2.9 Hz, 2 H, $SiCH_AH_BNH_X$), 4.31 (q, $^3J_{HH}$ = 7.0 Hz, 2 H, OC*H*CH$_3$), 6.0 (br s, 1 H, NH); ^{13}C NMR (CD_2Cl_2, 23 °C) δ 15.9 (NCC*C*H$_2$C), 19.5 (OCH*C*H$_3$), 20.1 (C*C*H$_3$), 20.4 (C*C*H$_3$), 30.9 (2 C, C*C*H$_3$), 38.1 (SiCH$_2$N), 39.4 (NC*C*H$_2$C), 39.5 (NC*C*H$_2$C), 65.6 (N*C*C$_3$), 66.0 (N*C*C$_3$), 70.1 (O*C*HCH$_3$), 177.2 (C═O); ^{29}Si NMR (CD_2Cl_2, 23 °C) −97.5. Anal. Calcd for $C_{16}H_{29}NO_6Si$: C, 53.46; H, 8.13; N, 3.90. Found: C, 53.2; H, 8.1; N, 3.8.

Preparation of (Λ,*S*,*S*)-Bis[3-phenyllactato(2−)-*O*^{1},*O*^{2}][(2,2,6,6-tetramethylpiperidinio)methyl]silicate−Acetonitrile (8a·CH$_3$CN). Compound **15** (500 mg, 1.82 mmol) was added at 20 °C to a stirred solution of (*S*)-3-phenyllactic acid (605 mg, 3.64 mmol) in acetonitrile (8 mL), and the mixture was stirred for 1 min and then kept undisturbed at this temperature for 1 h. The resulting precipitate was isolated by filtration, washed with acetonitrile (2 × 10 mL), and dried in vacuo (0.01 Torr, 20 °C, 1 h) to give **8a**·CH_3CN in 85% yield as a colorless crystalline solid (850 mg, 1.54 mmol); mp 170 °C (dec; loss of CH_3CN at 86 °C). ^{15}N VACP/MAS NMR (22 °C, ν_{rot} = 5 kHz) δ −291.4 (C_3NH); ^{29}Si VACP/MAS NMR (22 °C, ν_{rot} = 5 kHz) δ −95.3. Upon dissolution of **8a**·CH_3CN in CD_2Cl_2 (c = 48 mmol L^{-1}) at 23 °C, epimerization occurred (establishment of an equilibrium, with a molar ratio major isomer/minor isomer = 0.76:0.24). NMR data for the major isomer: ^1H NMR (CD_2Cl_2, 23 °C) 1.24 (s, 3 H, CCH_3), 1.31 (s, 3 H, CCH_3), 1.33 (s, 3 H, CCH_3), 1.42 (s, 3 H, CCH_3), 1.60−1.91 (m, 6 H, CCH_2C), 2.41 (δ_A) and 2.69 (δ_B) (AB part of an ABX system, $^2J_{AB}$ = 17.3 Hz, $^3J_{AX}$ = 4.2 Hz, $^3J_{BX}$ = 3.3 Hz, 2 H, $SiCH_AH_BNH_X$), 2.77 (δ_A), 3.10 (δ_B), and 4.27 (δ_X) (ABX system, $^2J_{AB}$ = 14.1 Hz, $^3J_{AX}$ = 8.5 Hz, $^3J_{BX}$ = 3.8 Hz, 6 H, $CCH_AH_BCH_X$), 5.7 (br s, 1 H, NH), 7.13−7.33 (m, 10 H, C_6H_5); ^{13}C NMR (CD_2Cl_2, 23 °C) δ 15.9 (NCC*C*H$_2$C), 20.0 (C*C*H$_3$), 20.3 (C*C*H$_3$), 30.0 (C*C*H$_3$), 30.5 (C*C*H$_3$), 37.4 (SiCH$_2$N), 39.3 (NC*C*H$_2$C), 39.4 (NC*C*H$_2$C), 40.9 (OCH*C*H$_2$C), 65.8 (N*C*C$_3$), 66.3 (N*C*C$_3$), 75.6 (O*C*HCH$_2$C), 126.8 (C4, C_6H_5), 128.5 (C2/C6, C_6H_5), 129.9 (C3/C5, C_6H_5), 138.5 (C1, C_6H_5), 175.9 (C═O); ^{29}Si NMR (CD_2Cl_2, 23 °C) δ −96.5. NMR data for the minor isomer: ^1H NMR (CD_2Cl_2, 23 °C) 1.23 (s, 3 H, CCH_3), 1.26 (s, 3 H, CCH_3), 1.28 (s, 3 H, CCH_3), 1.32 (s, 3 H, CCH_3), 1.60−1.91 (m, 6 H, CCH_2C), 2.26 (δ_A) and 2.74 (δ_B) (AB part of an ABX system, $^2J_{AB}$ = 17.0 Hz, $^3J_{AX}$ = 4.0 Hz, $^3J_{BX}$ = 3.6 Hz, 2 H, $SiCH_AH_BNH_X$), 2.77 (δ_A), 3.18 (δ_B), and 4.44 (δ_X) (ABX system, $^2J_{AB}$ = 14.1 Hz, $^3J_{AX}$ = 8.5 Hz, $^3J_{BX}$ = 3.6 Hz, 6 H, $CCH_AH_BCH_X$), 5.8 (br s, 1 H, NH), 7.13−7.33 (m, 10 H, C_6H_5); ^{13}C NMR (CD_2Cl_2, 23 °C) δ 15.9 (NCC*C*H$_2$C), 20.1 (C*C*H$_3$), 20.3 (C*C*H$_3$), 30.0 (C*C*H$_3$), 30.8 (C*C*H$_3$), 37.8 (SiCH$_2$N), 39.3 (NC*C*H$_2$C), 39.4 (NC*C*H$_2$C), 39.7 (OCH*C*H$_2$C), 65.8 (N*C*C$_3$), 66.3 (N*C*C$_3$), 75.1 (O*C*HCH$_2$C), 126.8 (C4, C_6H_5), 128.7 (C2/C6, C_6H_5), 129.7 (C3/C5, C_6H_5), 138.8 (C1, C_6H_5), 176.0 (C═O); ^{29}Si NMR (CD_2Cl_2, 23 °C) δ −96.5. Anal. Calcd for $C_{30}H_{40}N_2O_6Si$: C, 65.19; H, 7.29; N, 5.07. Found: C, 65.0; H, 7.2; N, 4.9.

Preparation of (Λ,*S*,*S*)-Bis[mandelato(2−)-*O*^{1},*O*^{2}][(2,2,6,6-tetramethylpiperidinio)methyl]silicate (9a). Compound **15** (800 mg, 2.90 mmol) was added at 20 °C to a stirred solution of (*S*)-mandelic acid (883 mg, 5.80 mmol) in acetonitrile (2 mL), and the mixture was then kept undisturbed at this temperature for 20 min. The resulting precipitate was isolated by filtration, washed with acetonitrile (2 × 10 mL), and dried in vacuo (0.01 Torr, 20 °C, 1 h) to give **9a** in 81% yield as a colorless crystalline solid (1.13 g, 2.34 mmol); mp 308 °C. ^{15}N VACP/MAS NMR (22 °C, ν_{rot} = 5 kHz) δ −290.5 (C_3NH); ^{29}Si VACP/MAS NMR (22 °C, ν_{rot} = 6.5 kHz) δ −94.5. Upon dissolution of **9a** in CD_2Cl_2 (c = 41 mmol L^{-1}) at 23 °C, epimerization occurred (establishment of an equilibrium, with a molar ratio major isomer/minor isomer = 0.93:0.07). NMR data for the major isomer: ^1H NMR (CD_2Cl_2, 23 °C) δ 1.34 (s, 3 H, CCH_3), 1.35 (s, 3 H, CCH_3), 1.41 (s, 3 H, CCH_3), 1.55 (s, 3 H, CCH_3), 1.59−1.91 (m, 6 H, CCH_2C), 2.64 (δ_A) and 2.90 (δ_B) (AB part of an ABX system, $^2J_{AB}$ = 17.4 Hz, $^3J_{AX}$ = 4.2 Hz, $^3J_{BX}$ = 3.3 Hz, 2 H, $SiCH_AH_BNH_X$), 5.2 (s, 2 H, OCHC), 5.9 (br s, 1 H, NH), 7.22−7.35 and 7.38−7.46 (m, 10 H, C_6H_5); ^{13}C NMR (CD_2Cl_2, 23 °C) δ 15.9 (NCC*C*H$_2$C), 20.1 (C*C*H$_3$), 20.3 (C*C*H$_3$), 30.0 (C*C*H$_3$), 30.5 (C*C*H$_3$), 37.4 (SiCH$_2$N), 39.1 (NC*C*H$_2$C), 39.2 (NC*C*H$_2$C), 66.0 (N*C*C$_3$), 66.5 (N*C*C$_3$), 76.4 (O*C*HC), 127.0 (C2/C6, C_6H_5), 128.2 (C4, C_6H_5), 128.5 (C3/C5, C_6H_5), 138.7 (C1, C_6H_5), 174.6 (C═O); ^{29}Si NMR (CD_2Cl_2, 23 °C) δ −95.9. NMR data for the minor isomer: ^1H NMR (CD_2Cl_2, 23 °C) δ 0.9 (s, 3 H, CCH_3), 1.19 (s, 3 H, CCH_3), 1.21 (s, 3 H, CCH_3), 1.24 (s, 3 H, CCH_3), 1.59−1.91 (m, 6 H, CCH_2C), 2.47 (δ_A) and 2.89 (δ_B) (AB part of an ABX system, $^2J_{AB}$ = 17.2 Hz, $^3J_{AX}$ = 4.1 Hz, $^3J_{BX}$ = 3.3 Hz, 2 H, $SiCH_AH_BNH_X$), 5.41 (s, 2 H, OCHC),

5.9 (br s, 1 H, NH), 7.28−7.43 and 7.58−7.63 (m, 10 H, C_6H_5); ^{13}C NMR (CD_2Cl_2, 23 °C) δ 15.9 (NCCCH_2C), 20.0 (CCH_3), 20.2 (CCH_3), 30.5 (CCH_3), 30.8 (CCH_3), 37.3 (SiCH_2N), 39.0 (NCCH_2C), 39.2 (NCCH_2C), 65.7 (NCC_3), 66.1 (NCC_3), 75.1 (OCHC), 126.6 (C2/C6, C_6H_5), 127.9 (C4, C_6H_5), 128.4 (C3/C5, C_6H_5), 138.7 (C1, C_6H_5), 174.6 (C=O); ^{29}Si NMR (CD_2Cl_2, 23 °C) −96.4. Anal. Calcd for $C_{26}H_{33}NO_6Si$: C, 64.57; H, 6.88.; N, 2.90. Found: C, 63.9; H, 6.9; N, 3.1.

Crystal Structure Analyses. Suitable single crystals of *rac*-**3**, **4b**, **5a**·CH_2Cl_2, *rac*-**6**, **7b**, **8a**·CH_3CN, and **9a** were isolated directly from the respective reaction mixtures (see Preparation). The crystals were mounted in inert oil (perfluoroalkyl ether, ABCR) on a glass fiber and then transferred to the cold nitrogen gas stream of the diffractometer (Stoe IPDS; graphite-monochromated Mo Kα radiation (λ = 0.710 73 Å)). All structures were solved by direct methods.[14] A riding model was employed in the refinement[15] of the C*H* hydrogen atoms, whereas the N*H* and O*H* hydrogen atoms were localized in difference Fourier syntheses and refined freely.

Computational Studies. Geometry optimizations of the anionic model species **10** (SCF/TZP+ level) and the zwitterions **(Δ)-11**, **12b**, and **13a** (SCF/TZP level) were performed using the TURBOMOLE program system (version 5.6).[16] Critical points of the potential energy surfaces were characterized as local minima (zero imaginary frequencies) and saddle points (one imaginary frequency), respectively, by calculation of the vibrational frequencies. The calculated energies include the zero-point vibrational energy obtained by SCF calculations and the single-point MP2 energy. The transition state **10D** was found using the module *statpt* implemented in TURBOMOLE.

The TZP (triple-ζ plus polarization) basis set given in ref 17 is suitable to describe molecules with moderately polarized chemical bonds. To gain a more accurate description of pentacoordinate silicon species containing distinctly polarized silicon-element bonds, the exponents of the most diffuse s, p, and d GTOs (Gauss-type orbitals) for Si, F, O, N, C, and H were additionally optimized at the SCF level. For this purpose, a TZP basis set optimization was performed for all atoms of the *Si*F_2ONC skeleton and for the ammonio-nitrogen atom of the zwitterion (ammoniomethyl)[ethene-1-aminato-2-olato(2−)]difluorosilicate (**16**) (model for the zwitterions **(Δ)-11**, **12b**, and **13a**).[18] Furthermore, a TZP basis set optimization with additional diffuse s and p functions (TZP+) was performed for the *Si*F_2ONH skeleton of the anion [ethene-1-aminato-2-olato(2−)]difluorohydridosilicate(1−) (**17**) (model for the anion **10**).[19] The carbon and hydrogen atoms in the outer spheres of the *Si*-coordination polyhedra of **16** and **17** were not considered in these TZP and TZP+ basis set optimizations. Comparison of the standard exponents and the optimized exponents of the TZP (**16**) and TZP+ (**17**) basis is given in Table 9.

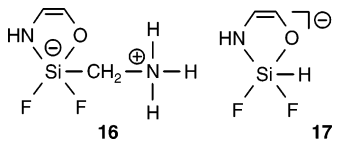

16 **17**

Table 9. Comparison of Standard Exponents and Optimized Exponents of the TZP[a] (TZP+)[b] Basis Used, Optimized for the Nitrogen Atom[c] of the Five-Membered Ring of the Zwitterionic Model Species **16** (Anionic Model Species **17**, with Additional Diffuse s and p Functions)

atom	function	TZP[d]	TZP_{opt}	atom	function	TZP+ [e]	$TZP+_{opt}$
N	η_{s8}	1.2525	1.2996	N	η_{s9}	0.5126	0.6241
	η_{s9}	0.5126	0.5147		η_{s10}	0.1794	0.2671
	η_{s10}	0.1794	0.1748		η_{s11}	0.0628	0.0933
	η_{p5}	0.4173	0.4044		η_{p6}	0.1430	0.2046
	η_{p6}	0.1430	0.1293		η_{p7}	0.0490	0.0995
	η_{d}	1.0000	0.9507		η_{d}	1.0000	0.9801

[a] TZP basis set: Si, (12s9p1d)/[7s5p1d]; F, O, and N, (10s6p1d)/[6s3p1d]; H, (5s1p)/[3s1p]. [b] TZP+ basis set: Si, (13s10p1d)/[8s6p1d]; F, O, and N, (11s7p1d)/[7s4p1d]; H, (6s2p)/[4s2p]. [c] Optimized exponents for Si, F, O, and the ammonio-nitrogen atom: see ref 21. [d] TZP basis sets taken from ref 17. [e] TZP+ basis sets generated from TZP basis with additional 1s and 1p functions via *define*.

Conclusions

With the synthesis of *rac*-**3**, **4b**, and **5a**·CH_2Cl_2 (*Si*O_2N_2C skeletons), members of a new class of pentacoordinate silicon complexes have been prepared. These compounds represent the first zwitterionic λ^5*Si*-silicates with bidentate ligands derived from α-amino acids. They can be regarded as nitrogen analogues of the zwitterionic λ^5*Si*-silicates *rac*-**6**, **7b**, and **8a**·CH_3CN (NH/O replacement) that contain bidentate ligands derived from α-hydroxycarboxylic acids.

The crystal structures of the respective NH/O analogues *rac*-**3**/*rac*-**6**, **4b**/**7b**, and **5a**/**8a** are similar, with distorted trigonal-bipyramidal *Si*-coordination polyhedra that contain the two carboxylato oxygen atoms in the axial positions. Upon dissolution in CD_2Cl_2 or $CDCl_3$ at room temperature, the enantiomerically and diastereomerically pure zwitterions **4b**, **5a**, **7b**, **8a**, and **9a** undergo a (Λ)/(Δ)-epimerization to give an equilibrium mixture of the respective (Λ,*S*,*S*)- and (Δ,*S*,*S*)-diastereomers. The chiral zwitterions with an *Si*O_2N_2C skeleton (**4**, **5**) are configurationally much more stable than those with an *Si*O_4C framework (**7**−**9**). Compound **4b**, with its (Δ,*S*,*S*)-configuration, was even demonstrated to be configurationally stable in CD_2Cl_2 at −20 °C over a period of 24 h. With these studies, a novel challenging field of silicon stereochemistry has been entered.

Compared to compounds *rac*-**6**, **7b**, **8a**, and **9a** (*Si*O_4C skeletons), the α-amino acid derivatives *rac*-**3**, **4b**, and **5a** are much more sensitive against water. According to these results, it is unlikely that pentacoordinate silicon species, with bidentate ligands derived from α-amino acids, play a role in silicon biochemistry (for speculations about the potential role of higher-coordinate silicon species in silicon biochemistry, see ref 20 and literature cited therein).

Acknowledgment. This work was supported by the Fonds der Chemischen Industrie.

Supporting Information Available: Tables of crystal data, structure solution and refinement, atomic coordinates, bond

(14) Sheldrick, G. M. SHELXS-97; University of Göttingen: Göttingen, Germany, 1997; Sheldrick, G. M. *Acta Crystallogr., Sect. A* **1990**, *46*, 467−473.
(15) Sheldrick, G. M. SHELX-97; University of Göttingen: Göttingen, Germany, 1997.
(16) Program system TURBOMOLE: Ahlrichs, R.; Bär, M.; Häser, M.; Horn, H.; Kölmel, C. *Chem. Phys. Lett.* **1989**, *162*, 165−169. Optimized TZP basis sets used for (Δ)-**11**, **12b**, and **13a**: Si, (12s9p1d)/[7s5p1d]; F, O, N, and C, (10s6p1d)/[6s3p1d]; H, (5s1p)/[3s1p]. Optimized TZP+ basis sets (with additional polarization functions) used for the anionic model species **10**: Si, (13s10p1d)/[8s6p1d]; F and O, (11s7p1d)/[7s4p1d]; H, (6s2p)/[4s2p].
(17) Schäfer, A.; Horn, H.; Ahlrichs, R. *J. Chem. Phys.* **1992**, *97*, 2571−2577.
(18) This particular molecule with an *Si*F_2ONC framework was chosen because it shall also serve as a model for theoretical studies of related zwitterionic monocyclic λ^5*Si*-silicates containing one bidentate ethene-1-aminato-2-olato ligand, two fluoro ligands, and one ammoniomethyl moiety bound to the *Si*-coordination center.
(19) This particular anion with an *Si*F_2ONH framework was chosen because it shall also serve as a model for theoretical studies of related anionic monocyclic λ^5*Si*-silicates containing one bidentate ethene-1-aminato-2-olato ligand, two fluoro ligands, and one hydrido ligand bound to the *Si*-coordination center.
(20) Tacke, R.; Penka, M.; Popp, F.; Richter, I. *Eur. J. Inorg. Chem.* **2002**, 1025−1028.
(21) Tacke, R.; Bertermann, R.; Biller, A.; Dannappel, O.; Penka, M.; Pülm, M.; Willeke, R. *Z. Anorg. Allg. Chem.* **2000**, *626*, 1159−1173.

lengths and angles, and anisotropic thermal parameters for *rac*-**3**, **4b**, **5a**·CH_2Cl_2, *rac*-**6**, **7b**, **8a**·CH_3CN, and **9a**. This material is available free of charge via the Internet at http://pubs.acs.org. In addition, crystallographic data (excluding structure factors) for the structures reported in this paper have been deposited with the Cambridge Crystallographic Data Centre as supplementary publication nos. CCDC-237671 (*rac*-**3**), CCDC-237672 (**4b**), CCDC-237673 (**5a**·CH_2Cl_2), CCDC-237674 (*rac*-**6**), CCDC-237675 (**7b**), CCDC-237676 (**8a**·CH_3CN), and CCDC-237670 (**9a**). Copies of the data can be obtained free of charge on application to CCDC, 12 Union Road, Cambridge CB2 1EZ, UK (Fax: (+44)1223/336033. E-mail: deposit@ccdc.cam.ac.uk).

JA047248Z